Wideband MIMO Mobile-to-Mobile Channels: Geometry-Based Statistical Modeling With Experimental Verification

Alenka G. Zajić, *Student Member, IEEE*, Gordon L. Stüber, *Fellow, IEEE*, Thomas G. Pratt, *Member, IEEE*, and Son T. Nguyen

***Abstract*—A 3-D reference model for wideband multiple-input multiple-output (MIMO) mobile-to-mobile (M-to-M) channels is reviewed along with its corresponding first- and second-order channel statistics. To validate the reference model, an experimental MIMO M-to-M channel-sounding campaign was conducted for M-to-M vehicular communication with vehicles that travel along surface streets and expressways in a metropolitan area. To compare the first- and second-order channel statistics that were obtained from the reference model with those obtained from the empirical measurements, a new maximum-likelihood-based stochastic estimator is derived to extract the relevant model parameters from the measured data. The measured data is processed and compared with the analytical results. The close agreement between the analytically and empirically obtained channel statistics confirms the utility of the proposed reference model and the method for estimating the model parameters.**

***Index Terms*—Channel sounding, mobile-to-mobile (M-to-M) channels, parameter estimation, wideband channel model.**

I. Introduction

MOBILE-TO-MOBILE (M-to-M) communications play an important role in mobile ad hoc wireless networks, intelligent transportation systems, and relay-based cellular networks. The statistical properties of M-to-M channels are quite different from conventional fixed-to-mobile cellular land mobile radio channels [1]. M-to-M communication systems are equipped with low-elevation antennas and have both the transmitter and receiver in motion. Akki and Haber [1] proposed a two-dimensional (2-D) reference model for single-input single-output (SISO) M-to-M Rayleigh fading channels. Simulation models for SISO M-to-M channels have been reported in [2]–[4]. Channel sounding measurements for narrowband and wideband SISO M-to-M channels have been reported in [5] and [6], respectively. The reference and simulation models for narrowband multiple-input multiple-output (MIMO) M-to-M channels have been proposed in [7] and [8], based on 2-D radio propagation. All these previously reported 2-D models are accurate only for certain environments, e.g., rural areas. To more appropriately model radio propagation in an urban M-to-M environment, we have recently proposed a three-dimensional (3-D) reference model for wideband MIMO M-to-M channels [9], [10]. We have also derived the first- and second-order statistics for the proposed models [9]–[11] along with simulation models [10], [12]. Note that the previously reported models for MIMO M-to-M channels characterize outdoor radio propagation, assuming that all rays are only double bounced. In contrast, our 3-D reference model constructs the input delay-spread function as a superposition of line of sight (LoS), single-bounced transmit, single-bounced receive, and double-bounced rays.

This paper verifies our 3-D wideband MIMO M-to-M reference model in [9] and [10] by using MIMO M-to-M channel measurements that were collected from vehicles that travel along surface streets near the Georgia Institute of Technology (Georgia Tech) campus and along Interstate highways near the Midtown Atlanta metropolitan area. First, we review our reference model along with its corresponding first- and second-order statistics. Then, we describe the measurement campaign and the data processing techniques for processing the measured data. To compare the first- and second-order channel statistics that were obtained from our reference model with those obtained from the empirical measurements, a new maximum likelihood (ML)-based stochastic estimator is derived to extract the parameters that are needed for the reference model from the measured data. The new estimator jointly estimates the parameters of the distribution functions used to characterize the azimuth angle of departure (AAoD), elevation angle of departure (EAoD), azimuth angle of arrival (AAoA), elevation angle of arrival (EAoA), and the parameters that specify the contribution of the single- and double-bounced rays to the total averaged received power. This estimator is an extension of the stochastic estimator

Manuscript received January 10, 2008; revised April 25, 2008 and June 1, 2008. First published June 7, 2008; current version published February 17, 2009. This work was prepared through collaborative participation in the Collaborative Technology Alliance for Communications and Networks sponsored by the U.S. Army Research Laboratory under Cooperative Agreement DAAD19-01-2-0011. The U.S. Government is authorized to reproduce and distribute reprints for Government purposes notwithstanding any copyright notation thereon. The views and conclusions contained in this document are those of the authors and should not be interpreted as representing the official policies, either expressed or implied, of the Army Research Laboratory or the U.S. Government. The review of this paper was coordinated by Dr. R. Qiu.

A. G. Zajić is with the Wireless Systems Laboratory, School of Electrical and Computer Engineering, Georgia Institute of Technology, Atlanta, GA 30332 USA (e-mail: alenka@ece.gatech.edu).

G. L. Stüber is with the School of Electrical and Computer Engineering, Georgia Institute of Technology, Atlanta, GA 30332 USA (e-mail: stuber@ece.gatech.edu).

T. G. Pratt is with the Software Radio Laboratory, Georgia Tech Research Institute, Georgia Institute of Technology, Atlanta, GA 30332 USA.

S. T. Nguyen is with the Army Research Laboratory, Adelphi, MD 20783 USA, and also with the Software Radio Laboratory, Georgia Tech Research Institute, Georgia Institute of Technology, Atlanta, GA 30332 USA (e-mail: Thomas.Pratt@gtri.gatech.edu).

Color versions of one or more of the figures in this paper are available online at http://ieeexplore.ieee.org.

Digital Object Identifier 10.1109/TVT.2008.928001

in [13], which only estimates the parameters of the distribution function for characterizing the AAoAs. The performance of the new estimator is evaluated by deriving the Cramér–Rao lower bound (CRLB) and by comparing the mean square error of the parameter estimates to the CRLB. Simulation results show that the proposed estimator has an asymptotically optimal performance, because it reaches the CRLB for a small number of samples. Finally, we compare the space–time–frequency correlation function (STF-CF), the space–Doppler power spectral density (sD-psd), the power space–delay spectral density (psds), and the envelope level crossing rate (LCR) obtained from the reference model with estimated parameters with those obtained from the measured data. The close agreement between the analytical and empirical curves confirms the utility of the proposed reference model and the methodology for extracting the model parameters from the measured data.

The remainder of this paper is organized as follows. For ease of reference, Section II reviews our 3-D wideband MIMO M-to-M reference model and its first- and second-order statistics, i.e., STF-CF, sD-psd, psds, and LCR. Section III describes the measurement campaign and the data processing techniques for processing the measured data. Section IV presents the new ML-based stochastic estimator. Section V compares the analytical and empirical results for sD-psd, psds, and LCR. Section VI provides some concluding remarks.

II. Geometry-Based Statistical Model for Wideband MIMO M-to-M Channels

This paper considers a wideband MIMO communication system with L_t transmit and L_r receive omnidirectional antenna elements. It is assumed that both the transmitter T_x and the receiver R_x are in motion and equipped with low-elevation antennas. The radio propagation occurs in outdoor metropolitan environments that are characterized by 3-D nonisotropic scattering with either LoS or non-LoS (NLoS) conditions between the T_x and R_x. The MIMO channel can be described by an $L_r \times L_t$ matrix $\mathbf{H}(t,\tau) = [h_{ij}(t,\tau)]_{L_r \times L_t}$ of the input delay-spread functions.

This section describes our 3-D reference model for wideband MIMO M-to-M multipath fading channels proposed in [9], [10]. The 3-D reference model is derived using our 3-D geometrical concentric-cylinders model. Fig. 1 shows the concentric-cylinders model with LoS, single-bounced transmit, single-bounced receive, and double-bounced rays for a MIMO M-to-M channel with $L_t = L_r = 2$ antenna elements. This elementary 2×2 antenna configuration will later be used to construct uniform linear antenna arrays with an arbitrary number of antenna elements. The concentric-cylinders model defines four vertical cylinders—two cylinders around the $\mathrm{T_x}$ and another two cylinders around the $\mathrm{R_x}$—as shown in Fig. 1. Around the $\mathrm{T_x}$, M fixed omnidirectional scatterers occupy a volume between cylinders of radii R_{t1} and R_{t2}. It is assumed that the M scatterers lie on L cylindric surfaces of radii $R_{t1} \leq R_t^{(l)} \leq R_{t2}$, where $1 \leq l \leq L$. The lth cylindric surface contains $M^{(l)}$ fixed omnidirectional scatterers, and the (m,l)th transmit scatterer is denoted by $S_T^{(m,l)}$, where $1 \leq m \leq M^{(l)}$. Similarly, around the R_x, N fixed omnidirectional scatterers occupy a volume

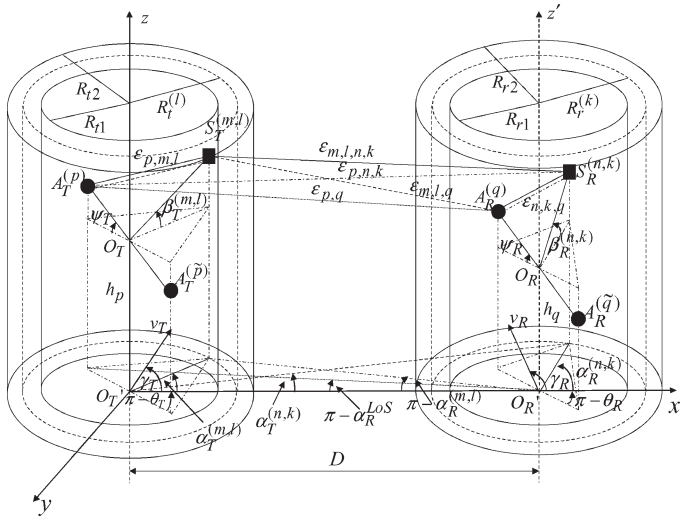

Fig. 1. Concentric-cylinders model with LoS, single-bounced transmit, single-bounced receive, and double-bounced rays for a MIMO M-to-M channel with $L_t = L_r = 2$ antenna elements.

between cylinders of radii R_{r1} and R_{r2}. It is assumed that the N scatterers lie on P cylindric surfaces of radii $R_{r1} \leq R_r^{(k)} \leq R_{r2}$, where $1 \leq k \leq P$. The kth cylindric surface contains $N^{(k)}$ fixed omnidirectional scatterers, and the (n,k)th receive scatterer is denoted by $S_R^{(n,k)}$, where $1 \leq n \leq N^{(k)}$. The distance between the centers of the $\mathrm{T_x}$ and $\mathrm{R_x}$ cylinders is D. It is assumed that the radii R_{t2} and R_{r2} are sufficiently smaller than the distance D (i.e., a local scattering condition). Furthermore, it is assumed that the distance D is smaller than $4R_{t1}R_{r1}L_r/(\lambda(L_t-1)(L_r-1))$ (i.e., the channel does not experience keyhole behavior [14]), where λ denotes the carrier wavelength. The spacing between antenna elements at the $\mathrm{T_x}$ and $\mathrm{R_x}$ is denoted by d_T and d_R, respectively. It is assumed that d_T and d_R are much smaller than the radii R_{t1} and R_{r1}. Angles θ_T and θ_R describe the orientation of the $\mathrm{T_x}$ and $\mathrm{R_x}$ antenna array in the xy plane, respectively, relative to the x-axis. Similarly, angles ψ_T and ψ_R describe the elevation of the $\mathrm{T_x}$'s antenna array and the $\mathrm{R_x}$'s antenna array relative to the xy plane, respectively. The $\mathrm{T_x}$ and $\mathrm{R_x}$ are moving with speed v_T and v_R. Angles γ_T and γ_R describe the moving directions of the $\mathrm{T_x}$ and $\mathrm{R_x}$ in the x–y plane, respectively, relative to the x-axis. The symbols $\epsilon_{p,m,l}$, $\epsilon_{m,l,q}$, $\epsilon_{p,n,k}$, $\epsilon_{n,k,q}$, $\epsilon_{m,l,n,k}$, and $\epsilon_{p,q}$ denote distances $A_T^{(p)} - S_T^{(m,l)}$, $S_T^{(m,l)} - A_R^{(q)}$, $A_T^{(p)} - S_R^{(n,k)}$, $S_R^{(n,k)} - A_R^{(q)}$, $S_T^{(m,l)} - S_R^{(n,k)}$, and $A_T^{(p)} - A_R^{(q)}$, respectively, as shown in Fig. 1. The symbols $\alpha_T^{(m,l)}$ and $\alpha_R^{(n,k)}$ denote AAoDs and AAoAs, respectively. Similarly, the symbols $\beta_T^{(m,l)}$ and $\beta_R^{(n,k)}$ denote EAoDs and EAoAs, respectively. Finally, the symbol α_{Rq}^{LoS} denotes the AAoAs of the LoS paths.

Observe from the 3-D geometrical model that some waves from the $\mathrm{T_x}$ antenna may directly traverse to the $\mathrm{R_x}$ antenna, whereas other waves are single-bounced at the $\mathrm{T_x}$, single-bounced at the $\mathrm{R_x}$, and/or double-bounced (i.e., the waves from the $\mathrm{T_x}$ antenna elements impinge on the scatterers that are located around the $\mathrm{T_x}$ and scatter from the scatterers that are located around the $\mathrm{R_x}$) before arriving at the $\mathrm{R_x}$ antenna. Hence, the input delay-spread function of the link $A_T^{(p)} - A_R^{(q)}$

can be written as a superposition of the LoS, single-bounced transmit, single-bounced receive, and double-bounced rays, i.e.,

$$h_{pq}(t,\tau)=h_{pq}^{SBT}(t,\tau)+h_{pq}^{SBR}(t,\tau)+h_{pq}^{DB}(t,\tau)+h_{pq}^{LoS}(t,\tau). \tag{1}$$

To simplify further analysis, we use the time-variant transfer function instead of the input delay-spread function. The time-variant transfer function is the Fourier transform of the input delay-spread function and can be written as [9]

$$T_{pq}(t,f)=\mathcal{F}_\tau\left\{h_{pq}(t,\tau)\right\}=T_{pq}^{SBT}(t,f)+T_{pq}^{SBR}(t,f)+T_{pq}^{DB}(t,f)+T_{pq}^{LoS}(t,f) \tag{2}$$

where the single-bounced transmit, single-bounced receive, double-bounced rays, and LoS components of the time-variant transfer function are, respectively

$$T_{pq}^{SBT}(t,f)=\sqrt{\frac{\eta_T\Omega_{pq}}{K+1}}\lim_{M\to\infty}\sum_{l=1}^{L}\sum_{m=1}^{M^{(l)}}\frac{\left(1-\frac{\gamma}{2}\frac{R_t^{(l)}}{D}\right)}{\sqrt{M}}$$
$$\times a_{p,m,l}^{SBT}b_{q,m,l}^{SBT}e^{j2\pi t f_{T\max}\cos\left(\alpha_T^{(m,l)}-\gamma_T\right)\cos\beta_T^{(m,l)}}$$
$$\times e^{j2\pi t f_{R\max}\left(\cos\gamma_R-\Delta_T^{(l)}\sin\gamma_R\sin\alpha_T^{(m,l)}\right)\cos\left(\Delta_T^{(l)}\beta_T^{(m,l)}+\Delta_H/D\right)}$$
$$\times e^{-j\frac{2\pi}{c_0\cos\beta_T^{(m,l)}}f\left[D+R_t^{(l)}\left(1-\cos\alpha_T^{(m,l)}\right)\right]+j\phi_{m,l}} \tag{3}$$

$$T_{pq}^{SBR}(t,f)=\sqrt{\frac{\eta_R\Omega_{pq}}{K+1}}\lim_{N\to\infty}\sum_{k=1}^{P}\sum_{n=1}^{N^{(k)}}\frac{\left(1-\frac{\gamma}{2}\frac{R_r^{(k)}}{D}\right)}{\sqrt{N}}$$
$$\times a_{p,n,k}^{SBR}b_{q,n,k}^{SBR}e^{j2\pi t f_{R\max}\cos\left(\alpha_R^{(n,k)}-\gamma_R\right)\cos\beta_R^{(n,k)}}$$
$$\times e^{j2\pi t f_{T\max}\left(\Delta_R^{(k)}\sin\gamma_T\sin\alpha_R^{(n,k)}+\cos\gamma_T\right)\cos\left(\Delta_R^{(k)}\beta_R^{(n,k)}-\Delta_H/D\right)}$$
$$\times e^{-j\frac{2\pi}{c_0\cos\beta_R^{(n,k)}}f\left[D+R_r^{(k)}\left(1+\cos\alpha_R^{(n,k)}\right)\right]+j\phi_{n,k}} \tag{4}$$

$$T_{pq}^{DB}(t,f)=\sqrt{\frac{\eta_{TR}\Omega_{pq}}{K+1}}\lim_{M,N\to\infty}\sum_{l,m=1}^{L,M^{(l)}}\sum_{k,n=1}^{P,N^{(k)}}a_{p,m,l}^{DB}b_{q,n,k}^{DB}$$
$$\times\frac{\left(1-\frac{\gamma}{2}\frac{R_t^{(l)}+R_r^{(k)}}{2D}\right)}{\sqrt{MN}}e^{j2\pi t f_{T\max}\cos\left(\alpha_T^{(m,l)}-\gamma_T\right)\cos\beta_T^{(m,l)}}$$
$$\times e^{j2\pi t f_{R\max}\cos\left(\alpha_R^{(n,k)}-\gamma_R\right)\cos\beta_R^{(n,k)}}$$
$$\times e^{-j\frac{2\pi}{c_0}f\left[D+\frac{R_t^{(l)}\left(1-\cos\alpha_T^{(m,l)}\right)}{\cos\beta_T^{(m,l)}}+\frac{R_r^{(k)}\left(1+\cos\alpha_R^{(n,k)}\right)}{\cos\beta_R^{(n,k)}}\right]+j\phi_{m,l,n,k}} \tag{5}$$

$$T_{pq}^{LoS}(t,f)=\sqrt{\frac{K\Omega_{pq}}{K+1}}e^{j2\pi t\left[f_{T\max}\cos\gamma_T+f_{R\max}\cos(\pi-\gamma_R)\right]}$$
$$\times e^{-j\frac{2\pi}{c_0}f\sqrt{D^2+\Delta_H^2}}e^{-j\frac{2\pi}{\lambda}D+j\frac{2\pi}{\lambda}(0.5L_t+0.5-p)d_T\cos\theta_T\cos\psi_T}$$
$$\times e^{j\frac{2\pi}{\lambda}(0.5L_r+0.5-q)d_R\cos\psi_R\cos(\pi-\theta_R)}. \tag{6}$$

In (3)–(6), K denotes the Rice factor (i.e., the ratio of LoS to scatter received power), γ is the path loss exponent, c_0 is the speed of light, $f_{T\max}=v_T/\lambda$ and $f_{R\max}=v_R/\lambda$ are the maximum Doppler frequencies associated with the $\mathrm{T_x}$ and $\mathrm{R_x}$, respectively, $\Delta_T^{(l)}=R_t^{(l)}/D$, $\Delta_R^{(k)}=R_r^{(k)}/D$, $\Delta_H=h_T-h_R$, $\Omega_{pq}=D^{-\gamma}P_{pq}\lambda^2/(4\pi)^2$, and P_{pq} is the power transmitted through the subchannel $A_T^{(p)}-A_R^{(q)}$. The parameters η_T, η_R, and η_{TR} specify the contribution of the single- and double-bounced rays to the total averaged power, i.e., these parameters satisfy $\eta_T+\eta_R+\eta_{TR}=1$. Furthermore, the parameters p and q take values from the sets $p\in\{1,\ldots,L_t\}$ and $q\in\{1,\ldots,L_r\}$. Finally, $a_{p,m,l}^{SBT}$, $b_{q,m,l}^{SBT}$, $a_{p,n,k}^{SBR}$, $b_{q,n,k}^{SBR}$, $a_{p,m,l}^{DB}$, and $b_{q,n,k}^{DB}$ are, respectively

$$a_{p,m,l}^{SBT}\approx e^{j\frac{2\pi}{\lambda}(0.5L_t+0.5-p)d_{Tx}\cos\alpha_T^{(m,l)}\cos\beta_T^{(m,l)}}$$
$$\times e^{j\frac{2\pi}{\lambda}(0.5L_t+0.5-p)\left[d_{Ty}\sin\alpha_T^{(m,l)}\cos\beta_T^{(m,l)}+d_{Tz}\sin\beta_T^{(m,l)}\right]} \tag{7}$$
$$b_{q,m,l}^{SBT}\approx e^{j\frac{2\pi}{\lambda}(0.5L_r+0.5-q)d_R\cos\psi_R\left[\Delta_T^{(l)}\sin\theta_R\sin\alpha_T^{(m,l)}-\cos\theta_R\right]}$$
$$\times e^{-j\frac{2\pi}{\lambda}\left(D+R_t^{(l)}\right)} \tag{8}$$
$$a_{p,n,k}^{SBR}\approx e^{j\frac{2\pi}{\lambda}(0.5L_t+0.5-p)d_T\cos\psi_T\left[\Delta_R^{(k)}\sin\theta_T\sin\alpha_R^{(n,k)}+\cos\theta_T\right]}$$
$$\times e^{-j\frac{2\pi}{\lambda}\left(D+R_r^{(k)}\right)} \tag{9}$$
$$b_{q,n,k}^{SBR}\approx e^{j\frac{2\pi}{\lambda}(0.5L_r+0.5-q)d_{Rx}\cos\alpha_R^{(n,k)}\cos\beta_R^{(n,k)}}$$
$$\times e^{j\frac{2\pi}{\lambda}(0.5L_r+0.5-q)\left[d_{Ry}\sin\alpha_R^{(n,k)}\cos\beta_R^{(n,k)}+d_{Rz}\sin\beta_R^{(n,k)}\right]} \tag{10}$$
$$a_{p,m,l}^{DB}\approx e^{j\frac{2\pi}{\lambda}(0.5L_t+0.5-p)d_{Tx}\cos\alpha_T^{(m,l)}\cos\beta_T^{(m,l)}}$$
$$\times e^{j\frac{2\pi}{\lambda}(0.5L_t+0.5-p)\left[d_{Ty}\sin\alpha_T^{(m,l)}\cos\beta_T^{(m,l)}+d_{Tz}\sin\beta_T^{(m,l)}\right]}$$
$$\times e^{-j\frac{2\pi}{\lambda}\left(D/2+R_t^{(l)}\right)} \tag{11}$$
$$b_{q,n,k}^{DB}\approx e^{j\frac{2\pi}{\lambda}(0.5L_r+0.5-q)d_{Rx}\cos\alpha_R^{(n,k)}\cos\beta_R^{(n,k)}}$$
$$\times e^{j\frac{2\pi}{\lambda}(0.5L_r+0.5-q)\left[d_{Ry}\sin\alpha_R^{(n,k)}\cos\beta_R^{(n,k)}+d_{Rz}\sin\beta_R^{(n,k)}\right]}$$
$$\times e^{-j\frac{2\pi}{\lambda}\left(D/2+R_r^{(k)}\right)} \tag{12}$$

where $d_{Tz}=d_T\sin\psi_T$, $d_{Tx}=d_T\cos\psi_T\cos\theta_T$, $d_{Ty}=d_T\cos\psi_T\sin\theta_T$, $d_{Rz}=d_R\sin\psi_R$, $d_{Rx}=d_R\cos\psi_R\cos\theta_R$, and $d_{Ry}=d_R\cos\psi_R\sin\theta_R$.

The model in [9] assumes that the angles of departure (i.e., $\alpha_T^{(m,l)}$ and $\beta_T^{(m,l)}$) and the angles of arrival (i.e., $\alpha_R^{(n,k)}$ and $\beta_R^{(n,k)}$) are independent random variables. Furthermore, it is assumed that the radii $R_t^{(l)}$ and $R_r^{(k)}$ are independent random variables. Finally, it is assumed that the phases $\phi_{m,l}$, $\phi_{n,k}$, and $\phi_{m,l,n,k}$ are random variables that were uniformly distributed on the interval $[-\pi,\pi)$ and independent of the angles of departure, the angles of arrival, and the radii of the cylinders. Using the aforementioned assumptions and the Central Limit Theorem [15], we can conclude that $T_{pq}^{SBT}(t,f)$, $T_{pq}^{SBR}(t,f)$, and $T_{pq}^{DB}(t,f)$ are independent complex Gaussian random processes with zero mean.

Several different scatterer distributions, e.g., uniform, Gaussian, Laplacian, and von Mises, are used in prior work to characterize the AAoD $\alpha_T^{(m,l)}$ and AAoA $\alpha_R^{(n,k)}$. In this paper, we use the von Mises probability density function (pdf), because it approximates many of the previously mentioned distributions and leads to closed-form solutions for many useful situations. The von Mises pdf is defined as [16]

$$f(\theta)=\exp\left[\kappa\cos(\theta-\mu)\right]/2\pi I_0(\kappa) \tag{13}$$

where $\theta \in [-\pi, \pi)$, $I_0(\cdot)$ is the zeroth-order modified Bessel function of the first kind, $\mu \in [-\pi, \pi)$ is the mean angle at which the scatterers are distributed in the x–y plane, and κ controls the spread of scatterers around the mean. When $\kappa = 0$, $f(\theta) = 1/(2\pi)$ is a uniform distribution that yields isotropic scattering in the horizontal plane. As κ increases, the scatterers become more clustered around angle μ, and the scattering becomes increasingly nonisotropic. Here, we denote the von Mises pdf for the $\mathrm{T_x}$ and $\mathrm{R_x}$ azimuth angles as $f(\alpha_T) = \exp[k_T \cos(\alpha_T - \mu_T)]/2\pi I_0(k_T)$ and $f(\alpha_R) = \exp[k_R \cos(\alpha_R - \mu_R)]/2\pi I_0(k_R)$, respectively. Prior work uses several different scatterer distributions, e.g., uniform, cosine, and Gaussian, to characterize the random EAoD $\beta_T^{(m,l)}$ and EAoA $\beta_R^{(n,k)}$. Here, we use the pdf [17] as follows:

$$f(\varphi) = \begin{cases} \frac{\pi}{4|\varphi_m|} \cos\left(\frac{\pi}{2}\frac{\varphi}{\varphi_m}\right), & |\varphi| \le |\varphi_m| \le \frac{\pi}{2} \\ 0, & \text{otherwise} \end{cases} \tag{14}$$

where φ_m is the maximum elevation angle and lies in the range $0^\circ \le |\varphi_m| \le 20^\circ$ [18]. Such elevation angles are typical for the "street canyon" type of propagation, which is prevalent in M-to-M communications where both the $\mathrm{T_x}$ and $\mathrm{R_x}$ are in motion and equipped with low-elevation antennas (e.g., two vehicles that drive along streets). We denote the pdf for the $\mathrm{T_x}$ and $\mathrm{R_x}$ elevation angles as $f(\beta_T) = \pi \cos(\pi\beta_T/(2\beta_{T_m}))/(4|\beta_{T_m}|)$ and $f(\beta_R) = \pi \cos(\pi\beta_R/(2\beta_{R_m}))/(4|\beta_{R_m}|)$, respectively. Finally, the radii $R_t^{(l)}$ and $R_r^{(k)}$ are characterized by the pdfs $f(R_t) = 2R_t/(R_{t2}^2 - R_{t1}^2)$ and $f(R_r) = 2R_r/(R_{r2}^2 - R_{r1}^2)$, respectively, [9]. For ease of reference, the parameters of the model are summarized in Table I, along with their nature, i.e., geometry-based, statistical, and estimated.

Based on the aforementioned 3-D reference model, we derived the STF-CF, sD-psd, psds, and LCR for a 3-D nonisotropic scattering environment [9]–[11]. These results are summarized in Appendix A and compared with the measured data in Sections IV and V.

TABLE I
DEFINITION OF THE PARAMETERS THAT WERE USED IN THE GEOMETRY-BASED STATISTICAL MODEL

D	The distance between the centers of the Tx and Rx cylinders.	Deterministic, geometry-based
d_T, d_R	The spacing between two adjacent antenna elements at the Tx and Rx, respectively.	Deterministic, geometry-based
θ_T, θ_R	The orientation of the Tx and Rx antenna array in the x-y plane (relative to the x-axis), respectively.	Deterministic, geometry-based
ψ_T, ψ_R	The elevation of the Tx's and Rx's antenna array relative to the x-y plane, respectively.	Deterministic, geometry-based
γ_T, γ_R	The moving directions of the Tx and Rx, in the x-y plane (relative to the x-axis), respectively.	Deterministic, geometry-based
h_T, h_R	The distances $d(O_T, O_T')$ and $d(O_R, O_R')$, respectively.	Deterministic, geometry-based
$f_{T\max}$, $f_{R\max}$	The maximum Doppler frequencies	Deterministic, calculated
$R_t^{(l)}$, $R_r^{(k)}$	The radius of the l^{th} Tx and k^{th} Rx cylinder, respectively.	Statistical, random variables
$\alpha_T^{(m,l)}$, $\alpha_R^{(n,k)}$	The azimuth angles of departure (AAoD) and the azimuth angles of arrival (AAoA), respectively.	Statistical, random variables
$\beta_T^{(m,l)}$, $\beta_R^{(n,k)}$	The elevation angles of departure (EAoD) and the elevation angles of arrival (EAoA), respectively.	Statistical, random variables
ϕ_m, ϕ_n, ϕ_{mn}	The phases	Statistical, random variables
k_T, k_R	The spread of scatterers around the mean; the parameter in the von Mises pdf.	Estimated from measurements or selected to characterize chosen propagation environment
μ_T, μ_R	The mean angle at which the scatterers are distributed in the x-y plane; the parameter in the von Mises pdf.	Estimated from measurements or selected to characterize chosen propagation environment
β_{Tm}, β_{Rm}	The maximum elevation angles	Estimated from measurements or selected to characterize chosen propagation environment
R_{t1}, R_{t2}, R_{r1}, R_{r2}	The min and max radii of the cylinders around the Tx and Rx, respectively.	Estimated from measurements or selected to characterize chosen propagation environment
η_T, η_R, η_{TR}	Specify how much the single- and double-bounced rays contribute in the total averaged power.	Estimated from measurements or selected to characterize chosen propagation environment

III. MEASUREMENT CAMPAIGN DESCRIPTION AND DATA PROCESSING

This section describes our MIMO M-to-M channel-sounding experimental campaign and the signal processing techniques for processing the collected data.

A. Measurement Campaign Description

The MIMO M-to-M channel-sounding experimental campaign was conducted along surface streets around the Georgia Tech campus and on the Interstate highways in the Midtown Atlanta metropolitan area. Major test assets that were associated with the campaign include two Econoline vans equipped with a power generator and rechargeable power supplies. Each van was equipped with a linear antenna array, which consists of four vertically polarized magnetic-mount 2.435 GHz antenna elements. The antenna elements were placed across the roof of the van from the passenger side to the driver side and spaced 2.943 wavelengths apart from each other.[1] The vans were usually driven in a convoy fashion (in the same lane and at the same speed), roughly 100–300 m apart and with speeds of up to 60 mi/h.

Fig. 2(a) depicts the block diagram for the MIMO transmitter system in the trailing vehicle. One rubidium clock provided a common 10 MHz reference for two Agilent E4438C signal generators. The third generator, i.e., an Agilent E4433B, synchronized the two E4438C signal generators. The arbitrary waveform feature of the E4438C signal generators was used to program orthogonal OFDM channel-sounding waveforms to support 2×4 MIMO channel matrix estimation. One source transmitted on the odd subcarriers, whereas the other source transmitted on the even subcarriers. An FFT size of $N = 256$ was used for the OFDM signal, with a sample rate of 18 million complex samples/s. The OFDM symbols were transmitted in a loop-back fashion, with a pulse repetition interval of 300 μs, which corresponds to a maximum resolvable Doppler shift of 3.3 kHz. The signal generator output signals were passed through linear amplifiers and were then coupled to two adjacent antenna elements in the antenna array.

[1]The separation between antenna elements was selected by the antenna designer and was 36.2 cm (i.e., 2.943 wavelengths).

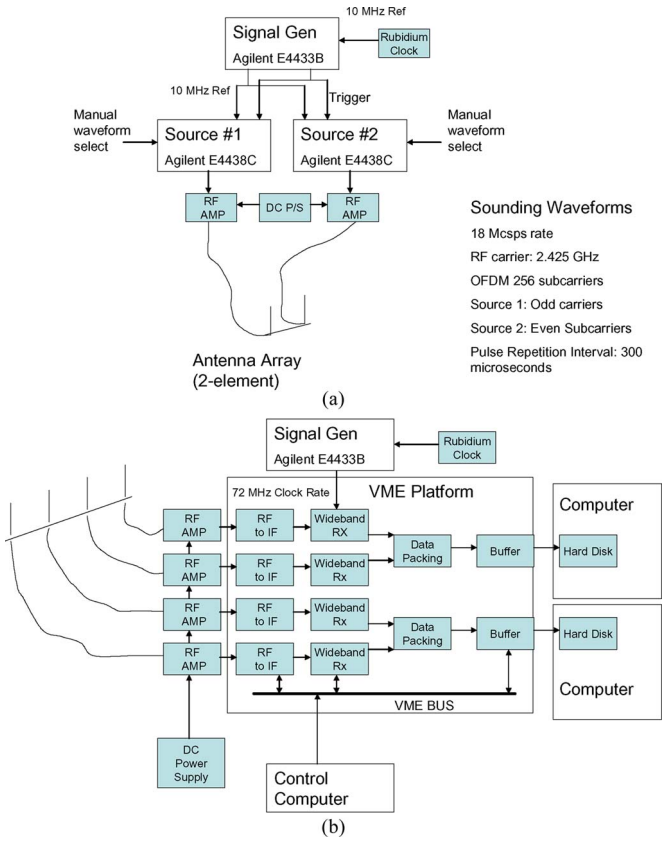

Fig. 2. Block diagram of (a) the MIMO transmitter system and (b) the MIMO receiver system.

Fig. 2(b) shows the block diagram for the MIMO receiver system in the leading vehicle. The signals were received by a four-element linear antenna array. Each of the received signals was coupled to a low-noise amplifier with 20 dB gain. The signals were then passed to VERSA-module Europe (VME) based radio frequency (RF)-to-intermediate frequency (IF) signal downconverters from Mercury Computer Systems, which converts the RF analog signal to an IF of 20 MHz. The resulting analog signals were sent pairwise into Pentek model 6235 wideband receiver boards that performed antialiasing filtering, analog-to-digital conversion at a 72 MHz complex sample rate, digital downconversion of the signals to complex baseband, and the $4:1$ decimation and filtering. The wideband receiver was clocked with an Agilent E4433B source with a 10 MHz reference from a rubidium clock source. The channels were synchronized pairwise. The use of the rubidium sources in both vans provided a mechanism for achieving frequency synchronization between the transmit and receive subsystems. The resulting baseband samples of each pairwise set from the digital downconverters were multiplexed and temporarily stored in a 2 GB buffer and were then streamed to a computer and stored on a hard disk. The buffer boards enabled 3 s contiguous snapshots to be collected from each of the four simultaneous channels at a sample rate of 18 million complex samples/channel/s. Due to processing memory constraints, the samples that were associated with any one snapshot were partitioned into 18 time-contiguous segments. Snapshots were collected at roughly 30 s apart.

TABLE II
DESCRIPTION OF THE MEASUREMENT CAMPAIGN

Carrier frequency	2.435 GHz
Tx antenna configuration	2.4 GHz magnetic mount antennas mounted in a 1x4 linear array on the van rooftop; 2 adjacent elements from the array were used for transmission
Rx antenna configuration	2.4 GHz magnetic mount antennas mounted in a 1x4 linear array on the van rooftop
Signal modulation	OFDM symbols with 256 subcarriers
Transmit sample rate (used to generate the OFDM signal)	18 MHz on a highway 36 MHz in an urban area
Transmit waveform pulse repetition interval	The pulse repetition interval of the sounding waveform was approximately 300 microseconds
Frequency synchronization	Rubidium clocks at the transmitter and the receiver
Data collection system	Pentek-based VME custom collection system with Mercury Computer Systems RF front ends; 4-channel receiver with pairwise sample synchronization
Data collection products at the receiver per snapshot (corresponding roughly to 3-second durations of contiguous data)	Approximately 55M contiguous complex baseband samples per antenna output
Collection scenario with mobile vans	Vans traveling 25 to 60 mph in the same direction and within 100 m to 300m apart on the I75 Expressway and along the streets around Georgia Tech

Fig. 3. Surface street area around the Georgia Tech campus, where the channel-sounding experimental campaign was conducted.

Channel-sounding waveforms were transmitted from the trailing vehicle, and the signals were received and recorded by the leading vehicle. Video cameras were used in the vehicles to provide indications of time, velocity, and location to support posttest processing of the collected data. The measurements typically included both LoS and NLoS conditions, as other vehicles and obstructions often masked the direct LoS. Details that are associated with the measurement campaign are summarized in Table II. Finally, Figs. 3 and 4 show photographs of the locations where the data used in this paper were collected.

B. Data Processing

Our wideband channel model is focused on characterizing the fast-fading characteristics of the channel. For fair comparison between our wideband channel model and the measured data, the slow-fading component of the measured signal envelope is removed using the local sliding window technique [19], where the sliding window length is set to 20λ.

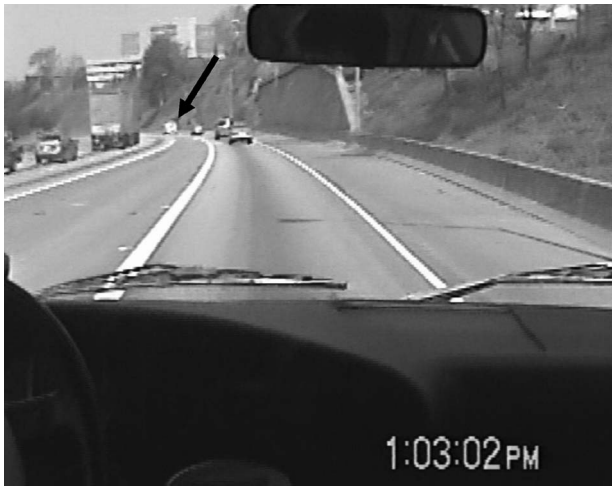

Fig. 4. Leading van, which was taken from the trailing van on the Interstate highway in the Midtown Atlanta metropolitan area.

From the measured input delay-spread function $\hat{h}_{pq}(n\Delta t_s, k\Delta\tau_s)$, we have calculated the STF-CF, sD-psd, psds, and LCR. The STF-CF is obtained as follows:

$$\tilde{R}_{pq,\tilde{p}\tilde{q}}(T\Delta t_s, F\Delta f_s) = (N_t N_\tau)^{-1} \sum_{n=0}^{N_t-1} \sum_{k=0}^{N_\tau-1} \times \hat{T}_{pq}(n\Delta t_s, k\Delta f_s)^* \hat{T}_{\tilde{p}\tilde{q}}([n+T]\Delta t_s, [k+F]\Delta f_s) \quad (15)$$

where Δt_s and N_t denote the sampling period and the number of samples with respect to the time variable t, $\Delta\tau_s$ and N_τ denote the sampling period and the number of samples with respect to the delay variable τ, $T \in \{0, \ldots, t_{\max} - 1\}$, $F \in \{0, \ldots, f_{\max} - 1\}$, $t_{\max} = \lceil 1/(B_d \Delta t_s) \rceil$, $f_{\max} = \lceil 1/(\Delta f_s \tau_{\max}) \rceil$, B_d is the Doppler spread, and $\tau_{\max}$ is the maximum relative delay.[2] Note that the maximum relative delay denotes a difference $\tau_1 - \tau_2$, where τ_1 is a delay when the psds achieves its maximum value, and τ_2 is a delay when the psds is 25 dB below its maximum value. The time-variant transfer function $\hat{T}_{pq}(n\Delta t_s, k\Delta f_s)$ is obtained from the input delay-spread function $\hat{h}_{pq}(n\Delta t_s, k\Delta\tau_s)$ using the fast Fourier transform. For fair comparison between the theoretical normalized STF-CF in (20) and the STF-CF from the measured data, we need to normalize the power of each measured subchannel $A_T^{(p)} - A_R^{(q)}$ to one. This normalization is performed as in (20), i.e.,

$$\hat{R}_{pq,\tilde{p}\tilde{q}}(T\Delta t_s, F\Delta f_s) = \frac{\tilde{R}_{pq,\tilde{p}\tilde{q}}(T\Delta t_s, F\Delta f_s)}{\sqrt{\mathrm{Var}\left[\hat{T}_{pq}(n\Delta t_s, k\Delta f_s)\right] \mathrm{Var}\left[\hat{T}_{\tilde{p}\tilde{q}}(n\Delta t_s, k\Delta f_s)\right]}}. \quad (16)$$

The sD-psd is obtained using the Welch algorithm [20]. The psds is obtained by averaging the squared magnitudes of the normalized input delay-spread function $\hat{h}_{pq}(n\Delta t_s, k\Delta\tau_s)$ over all times $n\Delta t_s$. Finally, the LCR $L(R)$ is obtained by counting how often (i.e., the number of times per second) the measured signal envelope crosses the level R in the positive direction.

[2]Operation $\lceil \cdot \rceil$ denotes rounding up to the next integer, B_d is estimated from the measured sD-psd, and $\tau_{\max}$ is estimated from the measured psds.

IV. Parameter Estimation

The parametric nature of our wideband channel model makes it adaptable to a variety of propagation environments. To verify our reference model with measured data, we need to estimate the model parameters from the measurements. The distances between antenna elements d_T and d_R, the difference in antenna heights Δ_H, the directions and speeds of the $\mathrm{T_x}$ and $\mathrm{R_x}$ (i.e., γ_T, γ_R, v_T, and v_R), the azimuth angles of the $\mathrm{T_x}$ and $\mathrm{R_x}$ antenna arrays (i.e., θ_T and θ_R), and the elevation angles of the $\mathrm{T_x}$ and $\mathrm{R_x}$ antenna arrays (i.e., ψ_T and ψ_R) are estimated from the antenna array geometry and the video camera recordings. The remaining parameters, i.e., the parameters in the von Mises pdfs k_T, μ_T, k_R, and μ_R, the parameters in the elevation angle pdfs, i.e., β_{T_m} and β_{R_m}, the parameters in the radii pdfs, i.e., R_{t1}, R_{t2}, R_{r1}, and R_{r2}, the parameters that specify the contribution of the single- and double-bounced rays to the total averaged power, i.e., η_T, η_R, and the Rice parameter K are estimated from the measured input delay-spread functions $\hat{h}_{pq}(n\Delta t_s, k\Delta\tau_s)$. Note that the parameter η_{TR} is equal to $1 - \eta_T - \eta_R$ and does not require estimation. First, the Rice factor is estimated using the moment method in [21]. Then, the parameters R_{t2} and R_{r2} are estimated from the measured psds by setting $R_{t2} = R_{r2} = c_0\tau_{\max}/2$, where $\tau_{\max}$ is the maximum relative delay, and c_0 is the speed of light. The parameters R_{t1} and R_{r1} are chosen to be $R_{t1} = R_{r1} = 0.1R_{t2}$. Finally, to estimate the parameters $\boldsymbol{\Theta} = [\beta_{T_m}, k_T, \mu_T, \beta_{R_m}, k_R, \mu_R, \eta_T, \eta_R]$, we propose a new ML-based stochastic estimator. This estimator is an extension of the stochastic estimator in [13], which only estimates the parameters in the von Mises pdf. In contrast to the estimator in [13], which estimates its parameters from the spatial correlation function, our estimator uses the STF-CF to estimate the parameters.

By observing that both the theoretical and measured input delay-spread functions are complex Gaussian random processes, we can estimate the parameters $\boldsymbol{\Theta} = [\beta_{T_m}, k_T, \mu_T, \beta_{R_m}, k_R, \mu_R, \eta_T, \eta_R]$ using an ML estimator with the log-likelihood function, i.e.,

$$\mathcal{L}\{\boldsymbol{\Theta}_{T,F}\} = -N_s \Big\{ \ln \pi^{L_r L_t} + \ln |\mathbf{R}(\boldsymbol{\Theta}_{T,F}, T\Delta t_s, F\Delta f_s)| + \mathrm{tr}\{\mathbf{R}(\boldsymbol{\Theta}_{T,F}, T\Delta t_s, F\Delta f_s)^{-1} \hat{\mathbf{R}}(T\Delta t_s, F\Delta f_s)\} \Big\} \quad (17)$$

where $\ln(\cdot)$ denotes the natural logarithm operation, $\mathrm{tr}(\cdot)$ denotes the matrix trace, $N_s = N_t N_\tau$ is the total number of samples, L_t and L_r denote the number of transmit and receive antennas, and $\boldsymbol{\Theta}_{T,F}$ denotes the vector of estimated parameters in the time and frequency instances $T\Delta t_s$ and $F\Delta f_s$. The elements $[\hat{\mathbf{R}}(T\Delta t_s, F\Delta f_s)]_{q+L_r(p-1),\tilde{q}+L_r(\tilde{p}-1)} = \hat{R}_{pq,\tilde{p}\tilde{q}}(T\Delta t_s, F\Delta f_s)$ of the $L_t L_r \times L_t L_r$ matrix of the measured correlation functions $\hat{\mathbf{R}}(T\Delta t_s, F\Delta f_s)$ are defined in (16), and the elements $[\mathbf{R}(\boldsymbol{\Theta}_{T,F}, T\Delta t_s, F\Delta f_s)]_{q+L_r(p-1),\tilde{q}+L_r(\tilde{p}-1)} = R_{pq,\tilde{p}\tilde{q}}(\boldsymbol{\Theta}_{T,F}, T\Delta t_s, F\Delta f_s)$ of the $L_t L_r \times L_t L_r$ matrix of the theoretical correlation functions $\mathbf{R}(\boldsymbol{\Theta}_{T,F}, n\Delta t_s, k\Delta f_s)$ are

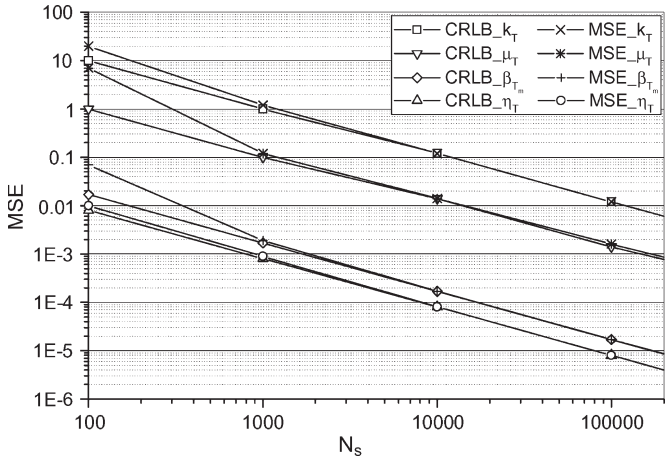

Fig. 5. Comparison of the MSE and the CRLB for the parameters $[\Theta_i]_{i=1}^4 = [\beta_{T_m}, k_T, \mu_T, \eta_T]$.

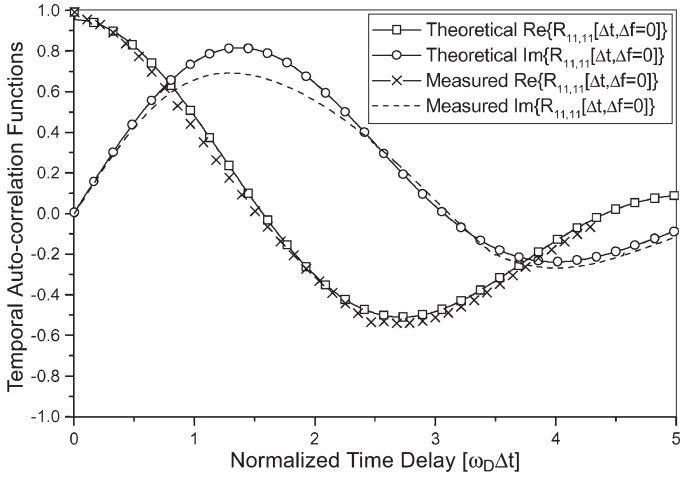

Fig. 6. Comparison of the theoretical and the measured temporal autocorrelation functions $R_{11,11}(\Delta t, \Delta f = 0)$.

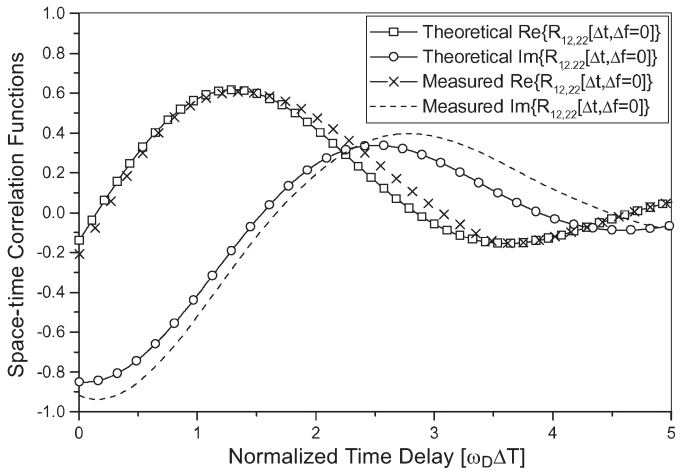

Fig. 7. Comparison of the theoretical and the measured space–time correlation functions $R_{12,22}(\Delta t, \Delta f = 0)$.

defined in (20). After removing the constant terms that are not dependent on the channel, the ML estimates are obtained as

$$\hat{\mathbf{\Theta}}_{T,F} = \arg\max_{\hat{\mathbf{\Theta}}_{T,F}} \Big\{ -\ln|\mathbf{R}(\mathbf{\Theta}_{T,F}, T\Delta t_s, F\Delta f_s)| - \mathrm{tr}\{\mathbf{R}(\mathbf{\Theta}_{T,F}, T\Delta t_s, F\Delta f_s)^{-1}\hat{\mathbf{R}}(T\Delta t_s, F\Delta f_s)\Big\} \quad (18)$$

with the constraint $\eta_T + \eta_R + \eta_{TR} = 1$. The expression in (18) is optimized using the sequential quadratic programming algorithm [22]. The final vector of estimated parameters $\mathbf{\Theta}$ is obtained as $\mathbf{\Theta} = (t_{\max} f_{\max})^{-1} \sum_{T=0}^{t_{\max}-1} \sum_{F=0}^{f_{\max}-1} \mathbf{\Theta}_{T,F}$.

To study the performance of the proposed estimator, we derive the CRLBs for the estimated parameters $\mathbf{\Theta} = [\Theta_i]_{i=1}^8 = [\beta_{T_m}, k_T, \mu_T, \beta_{R_m}, k_R, \mu_R, \eta_T, \eta_R]$. The CRLB bound of the estimated parameter Θ_i is the diagonal element of the inverse Fisher information matrix that corresponds to the parameter Θ_i. Appendix B shows that the (i,j)th element of the Fisher information matrix is

$$[\mathbf{F}(\mathbf{\Theta})]_{i,j} = -\mathrm{E}\left[\frac{\partial^2 \mathcal{L}(\mathbf{\Theta})}{\partial\Theta_i \partial\Theta_j}\right] = \frac{N_s}{t_{\max} f_{\max}} \sum_{T=0}^{t_{\max}-1} \sum_{F=0}^{f_{\max}-1} \times \mathrm{tr}\Big\{\mathbf{R}(\mathbf{\Theta}_{T,F}, T\Delta t_s, F\Delta f_s)^{-1}\mathbf{D}_{\Theta_j}(\mathbf{\Theta}_{T,F}, T\Delta t_s, F\Delta f_s) \times \mathbf{R}(\mathbf{\Theta}_{T,F}, T\Delta t_s, F\Delta f_s)^{-1}\mathbf{D}_{\Theta_i}(\mathbf{\Theta}_{T,F}, T\Delta t_s, F\Delta f_s)\Big\} \quad (19)$$

where $\mathbf{D}_{\Theta_i}(\mathbf{\Theta}_{T,F}, T\Delta t_s, F\Delta f_s)$ denotes the derivative $\partial\mathbf{R}(\mathbf{\Theta}_{T,F}, T\Delta t_s, F\Delta f_s)/\partial\Theta_i$ for $i \in \{1, \ldots, 8\}$ and are derived in (54)–(61).

To illustrate the performance of the proposed estimator, we compare the derived CRLB with the mean square error $\mathrm{MSE} = (\hat{\Theta}_i - \tilde{\Theta}_i)^2$ for the parameters $[\Theta_i]_{i=1}^8 = [\beta_{T_m}, k_T, \mu_T, \beta_{R_m}, k_R, \mu_R, \eta_T, \eta_R]$, where $\hat{\Theta}_i$ denotes the exact value, and $\tilde{\Theta}_i$ denotes the estimated value of the parameter Θ_i. The results that were obtained for the parameters $[\beta_{R_m}, k_R, \mu_R, \eta_R]$ are almost identical to those for the parameters $[\beta_{T_m}, k_T, \mu_T, \eta_T]$; therefore, Fig. 5 plots the CRLB and the MSE only for the parameters $[\Theta_i]_{i=1}^4 = [\beta_{T_m}, k_T, \mu_T, \eta_T]$. The curves in Fig. 5 are obtained with the estimated parameters $\beta_{Tm} = 5.1°$, $\beta_{Rm} = 10.2°$, $\mu_T = 31.3°$, $\mu_R = 141.7°$, $k_T = 12.5$, $k_R = 10.2$, $\eta_T = 0.213$, $\eta_R = 0.234$, $\eta_{TR} = 0.82$, $K = 2.41$, $R_{t1} = R_{r1} = 9.6$ m, $R_{t2} = R_{r2} = 96$ m and with the parameters $\theta_T = \theta_R = 0°$, $\psi_T = \psi_R = 0°$, $\gamma_T = \gamma_R = 90°$, $\Delta_H = 0$, $L_t = L_r = 2$, $d_T = d_R = 2.943\,\lambda$, $D = 300$ m, $\lambda = 0.123$ m, $\gamma = 4$, $f_{T\max} = f_{R\max} = 90.86$ Hz, which are obtained from the antenna geometry and propagation conditions. The simulation results show that the proposed estimator has asymptotically optimal performance, because it reaches the CRLB for a small number of samples, i.e., $N_s = 10^3$. Finally, Figs. 6–9 compare the theoretical and measured correlation functions. The theoretical correlation functions are obtained with the parameters in Fig. 5, whereas the measured correlation functions are obtained from the data that were collected on the urban surface street area in Fig. 3. The close agreement between the theoretical and empirical curves confirms the utility of the proposed estimator.

V. Reference Model Validation

In this section, we compare the theoretical results in Section II with those obtained from the measurement campaign described in Section III. The wideband channel measurements

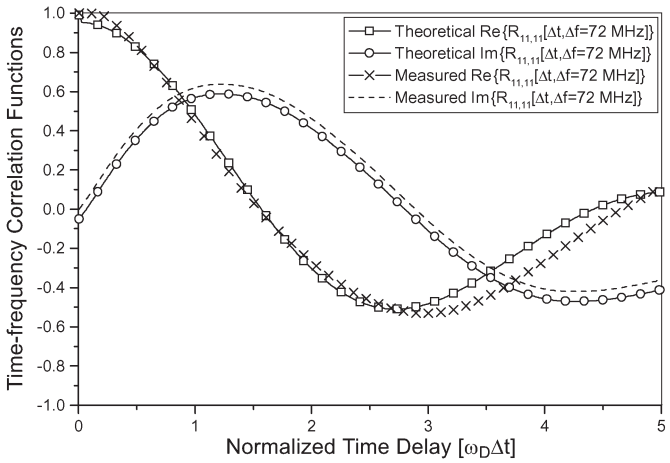

Fig. 8. Comparison of the theoretical and the measured time–frequency correlation functions $R_{11,11}(\Delta t, \Delta f = 72\ \text{Hz})$.

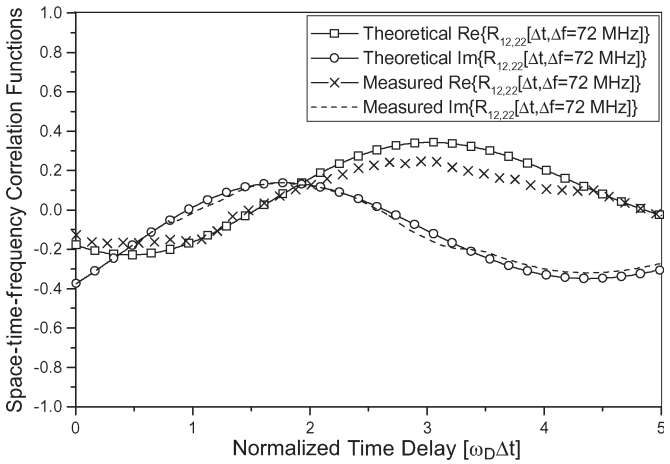

Fig. 9. Comparison of the theoretical and the measured STF-CFs $R_{12,22}(\Delta t, \Delta f = 72\ \text{Hz})$.

that were collected in the urban surface street area (as shown in Fig. 3) were performed at 2.435 GHz, and the maximum Doppler frequencies were $f_{T\max} = f_{R\max} = 90.86$ Hz. The distance between the $\mathrm{T_x}$ and $\mathrm{R_x}$ was approximately $D = 300$ m, and the moving directions were $\gamma_T = \gamma_R = 90^\circ$. Both $\mathrm{T_x}$ and $\mathrm{R_x}$ were equipped with two omnidirectional antenna elements with the azimuth and elevation angles $\theta_T = \theta_R = 0^\circ$ and $\psi_T = \psi_R = 0^\circ$, respectively. All antenna elements have the same height $\Delta_H = 0$, and the distance between the antenna elements is $d_T = d_R = 2.943\ \lambda$. It is assumed that the path loss exponent γ is 4, which is typical for radio propagation over a flat reflecting surface [24].

The reference model in (2)–(6) assumes an infinite number of scatterers around the $\mathrm{T_x}$ and $\mathrm{R_x}$, i.e., $M, N \to \infty$. Using the Central Limit Theorem [15], we can conclude that the theoretical time-variant transfer function $T_{pq}(t, f)$ is a complex Gaussian random process with mean $\mathrm{E}[T_{pq}(t, f)] = T_{pq}^{LoS}(t, f)$ and variance $\mathrm{Var}[T_{pq}(t, f)] = \Omega_{pq}/(K + 1)$. Before we compare the theoretical and measured sD-psd, psds, and LCR, we need to confirm that the measured time-variant transfer functions are also complex Gaussian random processes, with the means and variances being similar to

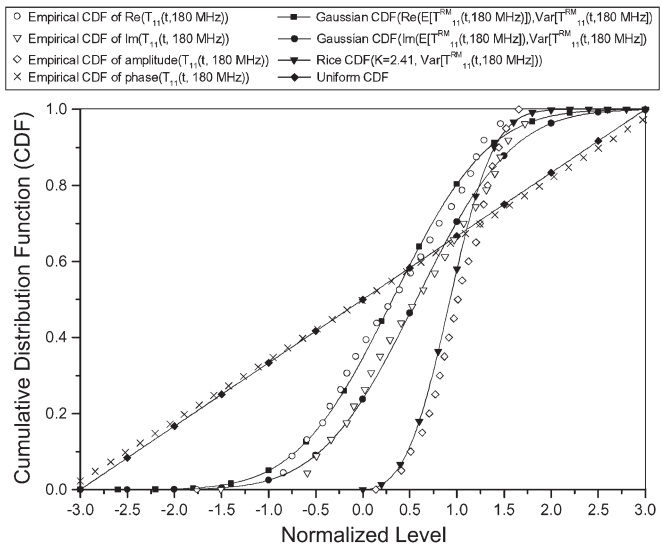

Fig. 10. Theoretical and empirical distribution functions of $h_{11}(t, \tau)$ in an urban surface street area.

those of the reference model. Fig. 10 compares the cumulative distribution functions (CDFs) of the real and imaginary components of the measured time-variant transfer function $\hat{T}_{11}(t, 180\ \text{MHz})$ with the CDFs of the real and imaginary components of the complex Gaussian process. The complex Gaussian process is obtained with mean $\mathrm{E}[T_{11}^{\mathrm{RM}}(t, 180\ \text{MHz})]$ and variance $\mathrm{Var}[T_{11}^{\mathrm{RM}}(t, 180\ \text{MHz})]$, respectively, where $T_{11}^{\mathrm{RM}}(t, 180\ \text{MHz})$ is the time-variant transfer function of the reference model. The results show that CDFs of the real and imaginary components of the measured time-variant transfer function $\hat{T}_{11}(t, 180\ \text{MHz})$ can closely be approximated by the Gaussian distributions, and the reference model and measured data have similar means and variances. Furthermore, the CDFs of the measured amplitude and phase can closely be approximated by a Rice and uniform distribution,[3] respectively. We have performed similar analysis (i.e., comparison of CDF functions and quantile–quantile plots) for all measured time-variant transfer functions, and similar results were observed.

Figs. 11–13 compare the theoretical and measured sD-psd, psds, and LCR for the urban surface street environment, respectively. The analytical curves are obtained with the parameters $\beta_{Tm} = 5.1^\circ$, $\beta_{Rm} = 10.2^\circ$, $\mu_T = 73.3^\circ$, $\mu_R = 264.7^\circ$, $k_T = 5.7$, $k_R = 6.4$, $\eta_T = 0.043$, $\eta_R = 0.137$, $\eta_{TR} = 0.82$, $R_{t1} = R_{r1} = 9.6$ m, $R_{t2} = R_{r2} = 96$ m, and $K = 2.41$. These parameters are estimated from the measured data, as described in Section IV. The parameters γ, D, γ_T, γ_R, θ_T, θ_R, ψ_T, ψ_R, d_T, d_R, Δ_H, $f_{T\max}$, and $f_{R\max}$ are selected to match the aforementioned measurement conditions. Figs. 11–13 show close agreement between the theoretical and empirical curves. Our results for urban surface street environments show that double-bounced rays bear more energy than the single-bounced rays. In addition, note that the estimated scattering radii $R_{t2} = R_{r2} = 96$ m are sufficiently small compared with the distance $D = 300$ m by which the local scattering condition is satisfied.

[3]With nonisotropic scattering, the phase may not be uniformly distributed.

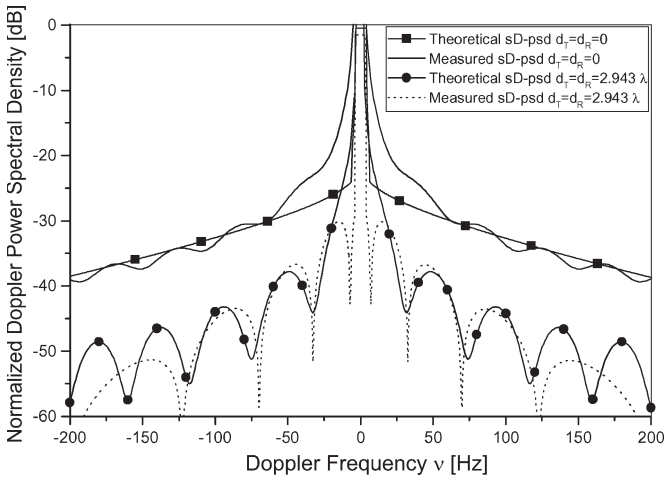

Fig. 11. Theoretical and measured sD-psd in an urban surface street area.

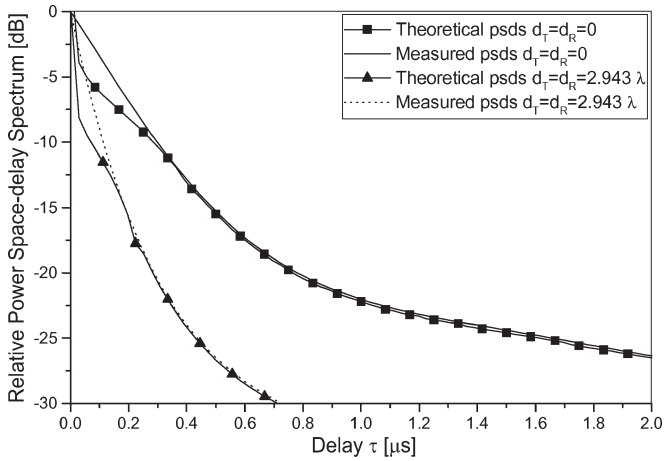

Fig. 12. Theoretical and measured psds in an urban surface street area.

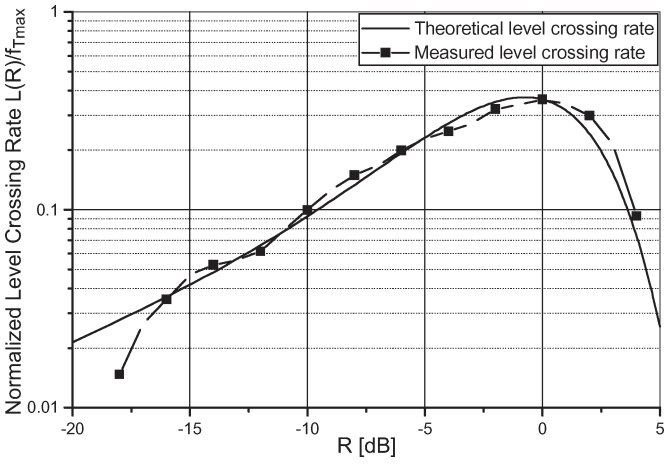

Fig. 13. Theoretical and measured LCR in an urban surface street area.

Finally, we note that channel-sounding measurements for narrowband and wideband SISO M-to-M channels in [5] and [6], similar to our theoretical results, show no oscillating pattern in the Doppler power spectrum. The oscillating pattern in our measurements for the case $d_T = d_R = 0$ may appear, because it is not a true SISO scenario, where only one transmit and one receive antenna are active. We have performed MIMO M-to-M

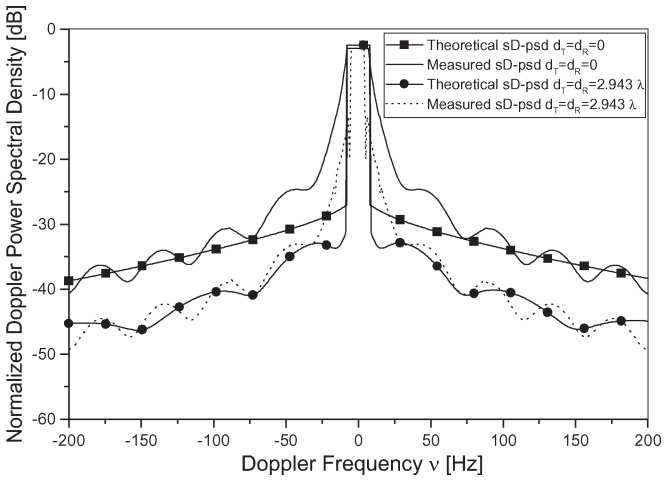

Fig. 14. Theoretical and measured sD-psd on an Interstate highway.

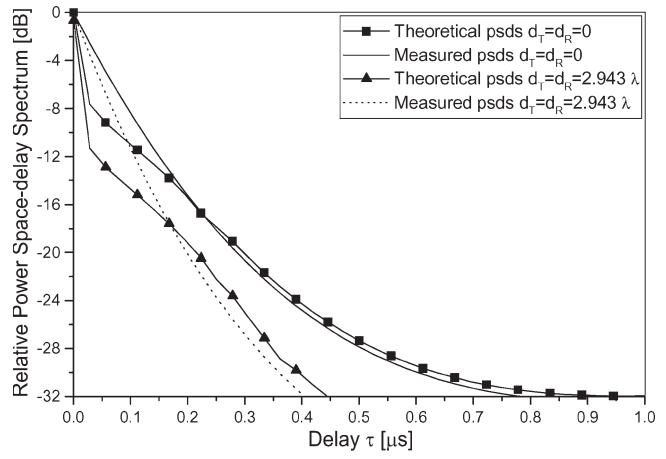

Fig. 15. Theoretical and measured psds on an Interstate highway.

channel measurements and calculated the SISO Doppler spectrum using the input delay-spread function $h_{11}(t, \tau)$. There may be a small degree of coupling with the other active antennas, which is manifested as the oscillating pattern in the Doppler power spectrum for $d_T = d_R = 0$. Another explanation may be the presence of moving scatterers (i.e., vehicles), whereas our model assumes stationary scatterers. The measurements in [6] were conducted at nighttime with very little road traffic.

The wideband channel measurements, which were collected on the Interstate highway (as shown in Fig. 4), were performed at 2.435 GHz, and the maximum Doppler frequencies were $f_{T\max} = f_{R\max} = 181.72$ Hz. The distance between the $\mathrm{T_x}$ and $\mathrm{R_x}$ was approximately $D = 180$ m, and the moving directions were $\gamma_T = \gamma_R = 90^\circ$. The $\mathrm{T_x}$ was equipped with two omnidirectional antenna elements, and the $\mathrm{R_x}$ was equipped with four omnidirectional antenna elements. The antenna array elements at both vehicles have the azimuth and elevation angles $\theta_T = \theta_R = 0^\circ$ and $\psi_T = \psi_R = 0^\circ$, respectively. All antenna elements have the same height $\Delta_H = 0$, and the distance between the antenna elements is $d_T = d_R = 2.943\ \lambda$. The path loss exponent γ is set to 4.

Figs. 14–16 compare the theoretical and measured sD-psd, psds, and LCR, respectively, on the Interstate highway. The analytical curves are obtained with the parameters $\beta_{Tm} = 7.4^\circ$,

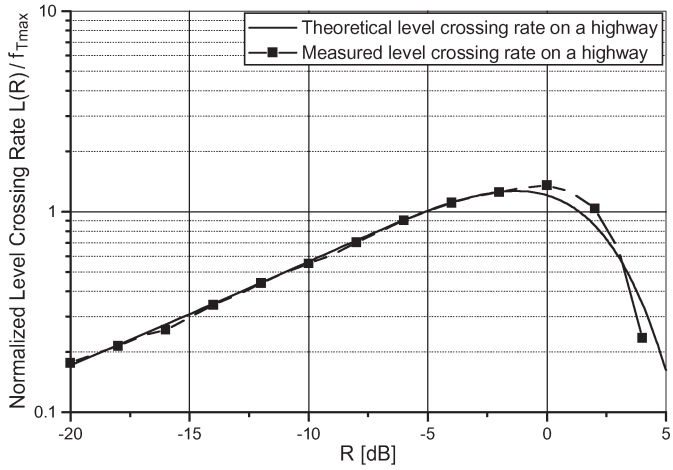

Fig. 16. Theoretical and measured LCR on an Interstate highway.

$\beta_{Rm} = 8.3°$, $\mu_T = 101.4°$, $\mu_R = 281.5°$, $k_T = 5.5$, $k_R = 5.2$, $\eta_T = 0.358$, $\eta_R = 0.288$, $\eta_{TR} = 0.354$, $R_{t1} = R_{r1} = 4.5$ m, $R_{t2} = R_{r2} = 45$ m, and $K = 1.29$. These parameters are estimated as described in Section IV. The remaining parameters D, $\gamma, \gamma_T, \gamma_R, \theta_T, \theta_R, \psi_T, \psi_R, d_T, d_R, \Delta_H, f_{T\max}$, and $f_{R\max}$ are selected as in the aforementioned highway measurement setup. Figs. 14–16 show close agreement between the theoretical and empirical curves. In this set of data, the single-bounced rays are more dominant than the double-bounced rays. This effect can be explained by the fact that both vans were in the rightmost lane and were very close to the sound blockers on the edge of the highway (see Fig. 4). Finally, the estimated scattering radii $R_{t2} = R_{r2} = 45$ m are sufficiently small compared to the distance $D = 180$ m that the local scattering condition is satisfied.

By analyzing the data that were collected at four different locations along the highway, we have observed that, if the vehicles are driven in the rightmost or the leftmost lane and are close to large objects, e.g., highway dividers or sound blockers, on the edge of the highway, single-bounced rays bear more energy than double-bounced rays. However, if the vehicles are driven in the middle lanes of the highway, double-bounced rays are prevalent.

Figs. 10–16 show close agreement between the theoretical and empirical curves. These results confirm the utility of the proposed model. Based on the results, we can observe that, in the urban surface street area, double-bounced rays bear more energy than single-bounced rays, whereas on the highway, single-bounced rays may be prevalent.

VI. Concluding Remarks

This paper has reviewed a 3-D reference model for wideband MIMO M-to-M channels along with the first- and second-order channel statistics. To validate this model, a MIMO M-to-M channel-sounding experimental campaign has been conducted in the Atlanta metropolitan area. To compare the analytical and empirical results, a new ML-based stochastic estimator has been proposed. The new estimator jointly estimates the parameters of the distribution functions to characterize the AAoD, EAoD, AAoA, EAoA, and the parameters that specify the contribution of the single- and double-bounced rays to the total averaged received power. The performance of the new estimator has been studied by deriving the CRLB and comparing the mean square error of the estimates to the CRLB. The simulations showed that the proposed estimator has asymptotically optimal performance, because it reaches the CRLB for a small number of samples. Finally, the measured data has been processed and compared with the analytical predictions. The close agreement between the analytical and empirical curves confirms the utility of the proposed reference model and methodology for extracting model parameters from the measured data.

Finally, we have noted that single-bounced rays and double-bounced rays have significantly different statistical properties, because the angles of departure of double-bounced rays are independent of their angles of arrival, whereas the angles of arrival of single-bounced rays are dependent on their angles of departure. On the other hand, the angles of departure of triple- or higher order-bounced rays, which are similar to double-bounced rays, are independent of their angles of arrival. Therefore, triple- or higher order-bounced rays have statistical properties that are very similar to those of the double-bounced rays and can be approximated as double-bounced rays.

Appendix A
Statistical Properties of Wideband MIMO M-to-M Channels

A. STF-CF

The normalized STF-CF between the two time-variant transfer functions in (2), i.e., $T_{pq}(t,f)$ and $T_{\tilde{p}\tilde{q}}(t,f)$, is defined as

$$R_{pq,\tilde{p}\tilde{q}}(\Delta t, \Delta f) = \frac{\mathrm{E}\left[T_{pq}(t,f)^* T_{\tilde{p}\tilde{q}}(t+\Delta t, f+\Delta f)\right]}{\sqrt{\mathrm{Var}\left[T_{pq}(t,f)\right]\mathrm{Var}\left[T_{\tilde{p}\tilde{q}}(t,f)\right]}} \quad (20)$$

where $(\cdot)^*$ denotes a complex conjugate operation, $\mathrm{E}[\cdot]$ is the statistical expectation operator, $\mathrm{Var}[\cdot]$ is the statistical variance operator, $p, \tilde{p} \in \{1, \ldots, L_t\}$, and $q, \tilde{q} \in \{1, \ldots, L_r\}$. $T_{pq}^{SBT}(t,f)$, $T_{pq}^{SBR}(t,f)$, and $T_{pq}^{DB}(t,f)$ are independent complex Gaussian random processes with zero mean, and therefore, (20) can be simplified to

$$R_{pq,\tilde{p}\tilde{q}}(\Delta t, \Delta f) = R_{pq,\tilde{p}\tilde{q}}^{SBT}(\Delta t, \Delta f) + R_{pq,\tilde{p}\tilde{q}}^{SBR}(\Delta t, \Delta f) + R_{pq,\tilde{p}\tilde{q}}^{DB}(\Delta t, \Delta f) + R_{pq,\tilde{p}\tilde{q}}^{LoS}(\Delta t, \Delta f) \quad (21)$$

where $R_{pq,\tilde{p}\tilde{q}}^{SBT}(\Delta t, \Delta f)$, $R_{pq,\tilde{p}\tilde{q}}^{SBR}(\Delta t, \Delta f)$, $R_{pq,\tilde{p}\tilde{q}}^{DB}(\Delta t, \Delta f)$, and $R_{pq,\tilde{p}\tilde{q}}^{LoS}(\Delta t, \Delta f)$ denote the normalized STF-CFs of the single-bounced transmit, single-bounced receive, double-bounced, and LoS components, respectively. In [9], it is shown that the STF-CFs of the single-bounced transmit, single-bounced receive, double-bounced, and LoS components, respectively, can closely be approximated as

$$R_{pq,\tilde{p}\tilde{q}}^{SBT}(\Delta t, \Delta f) \approx \frac{\mathrm{E}\left[T_{pq}^{SBT}(t,f)^* T_{\tilde{p}\tilde{q}}^{SBT}(t+\Delta t, f+\Delta f)\right]}{\Omega_{pq}/(1+K)} \approx \frac{\cos\left(\frac{2\pi}{\lambda}\beta_{Tm}(p-\tilde{p})d_{Tz}\right)}{1-\left(\frac{4\beta_{Tm}(p-\tilde{p})d_{Tz}}{\lambda}\right)^2} e^{-j\frac{2\pi}{\lambda}(q-\tilde{q})d_{Rx} - j2\pi\Delta t f_{R\max}\cos\gamma_R}$$

$$\times \frac{\eta_T}{I_0(k_T)} \int_{R_{t1}}^{R_{t2}} \left(1-\gamma\frac{R_t}{D}\right) e^{-j\frac{2\pi}{c_0}\Delta f(D+R_t)} \frac{2R_t}{R_{t2}^2-R_{t1}^2} \times I_0\left(\sqrt{x_{SBT}^2+y_{SBT}^2}\right) dR_t \quad (22)$$

$$R_{pq,\tilde{p}\tilde{q}}^{SBR}(\Delta t,\Delta f) \approx \frac{\mathrm{E}\left[T_{pq}^{SBR}(t,f)^* T_{\tilde{p}\tilde{q}}^{SBR}(t+\Delta t,f+\Delta f)\right]}{\Omega_{pq}/(1+K)}$$
$$\approx \frac{\cos\left(\frac{2\pi}{\lambda}\beta_{Rm}(q-\tilde{q})d_{Rz}\right)}{1-\left(\frac{4\beta_{Rm}(q-\tilde{q})d_{Rz}}{\lambda}\right)^2} e^{j\frac{2\pi}{\lambda}(p-\tilde{p})d_{Tx}+j2\pi\Delta t f_{T\max}\cos\gamma_T} \times \frac{\eta_R}{I_0(k_R)} \int_{R_{r1}}^{R_{r2}} \left(1-\gamma\frac{R_r}{D}\right) e^{-j\frac{2\pi}{c_0}\Delta f(D+R_r)} \frac{2R_r}{R_{r2}^2-R_{r1}^2} \times I_0\left(\sqrt{x_{SBR}^2+y_{SBR}^2}\right) dR_r \quad (23)$$

$$R_{pq,\tilde{p}\tilde{q}}^{DB}(\Delta t,\Delta f) \approx \frac{\mathrm{E}\left[T_{pq}^{DB}(t,f)^* T_{\tilde{p}\tilde{q}}^{DB}(t+\Delta t,f+\Delta f)\right]}{\Omega_{pq}/(1+K)}$$
$$\approx A_{DB} \int_{R_{t1}}^{R_{t2}} 2e^{-j\frac{2\pi}{c_0}\Delta f R_t} R_t I_0\left(\sqrt{x_{DB}^2+y_{DB}^2}\right) dR_t \times \int_{R_{r1}}^{R_{r2}} e^{-j\frac{2\pi}{c_0}\Delta f R_r} R_r I_0\left(\sqrt{w_{DB}^2+z_{DB}^2}\right)\left(1-\gamma\frac{R_r}{D}\right) dR_r + A_{DB} \int_{R_{r1}}^{R_{r2}} 2e^{-j\frac{2\pi}{c_0}\Delta f R_r} R_r I_0\left(\sqrt{w_{DB}^2+z_{DB}^2}\right) dR_r \times \int_{R_{t1}}^{R_{t2}} e^{-j\frac{2\pi}{c_0}\Delta f R_t} R_t I_0\left(\sqrt{x_{DB}^2+y_{DB}^2}\right)\left(1-\gamma\frac{R_t}{D}\right) dR_t \quad (24)$$

$$R_{pq,\tilde{p}\tilde{q}}^{LoS}(\Delta t,\Delta f) \approx \frac{\mathrm{E}\left[T_{pq}^{LoS}(t,f)^* T_{\tilde{p}\tilde{q}}^{LoS}(t+\Delta t,f+\Delta f)\right]}{\Omega_{pq}/(K+1)}$$
$$\approx K e^{j\frac{2\pi}{\lambda}[(p-\tilde{p})d_{Tx}-(q-\tilde{q})d_{Rx}]+j2\pi\Delta t[f_{T\max}\cos\gamma_T - f_{R\max}\cos\gamma_R]} \times e^{-j\frac{2\pi}{c_0}\Delta f\sqrt{D^2+\Delta_H^2}} \quad (25)$$

where parameters $x_{SBT}, y_{SBT}, x_{SBR}, y_{SBR}, x_{DB}, y_{DB}, z_{DB}$, w_{DB}, and A_{DB} are

$$x_{SBT} \approx j2\pi(p-\tilde{p})d_{Tx}/\lambda + j2\pi\Delta t f_{T\max}\cos\gamma_T + k_T\cos\mu_T + j2\pi\Delta f R_t/c_0 \quad (26)$$

$$y_{SBT} \approx j2\pi\left[(p-\tilde{p})d_{Ty}/\lambda + (q-\tilde{q})d_{Ry}\Delta_T\right] + k_T\sin\mu_T + j2\pi\Delta t(f_{T\max}\sin\gamma_T + f_{R\max}\Delta_T\sin\gamma_R) \quad (27)$$

$$x_{SBR} \approx j2\pi(q-\tilde{q})d_{Rx}/\lambda + j2\pi\Delta t f_{R\max}\cos\gamma_R + k_R\cos\mu_R - j2\pi\Delta f R_r/c_0 \quad (28)$$

$$y_{SBR} \approx j2\pi\left[(q-\tilde{q})d_{Ry}/\lambda + (p-\tilde{p})d_{Ty}\Delta_R\right] + k_R\sin\mu_R + j2\pi\Delta t(f_{R\max}\sin\gamma_R + f_{T\max}\Delta_R\sin\gamma_T) \quad (29)$$

$$x_{DB} \approx j2\pi(p-\tilde{p})d_{Tx}/\lambda + j2\pi\Delta t f_{T\max}\cos\gamma_T + k_T\cos\mu_T + j2\pi\Delta f R_t/c_0 \quad (30)$$

$$y_{DB} \approx j2\pi(p-\tilde{p})d_{Ty}/\lambda + j2\pi\Delta t f_{T\max}\sin\gamma_T + k_T\sin\mu_T \quad (31)$$

$$z_{DB} \approx j2\pi(q-\tilde{q})d_{Rx}/\lambda + j2\pi\Delta t f_{R\max}\cos\gamma_R + k_R\cos\mu_R - j\frac{2\pi}{c_0}\Delta f R_r \quad (32)$$

$$w_{DB} \approx j2\pi(q-\tilde{q})d_{Ry}/\lambda + j2\pi\Delta t f_{R\max}\sin\gamma_R + k_R\sin\mu_R \quad (33)$$

$$A_{DB} = \frac{\eta_{TR}}{I_0(k_T)I_0(k_R)} \frac{\cos\left(\frac{2\pi}{\lambda}\beta_{Tm}(p-\tilde{p})d_{Tz}\right)}{1-\left(\frac{4\beta_{Tm}(p-\tilde{p})d_{Tz}}{\lambda}\right)^2} \times \frac{\cos\left(\frac{2\pi}{\lambda}\beta_{Rm}(q-\tilde{q})d_{Rz}\right)}{1-\left(\frac{4\beta_{Rm}(q-\tilde{q})d_{Rz}}{\lambda}\right)^2} \frac{e^{-j2\pi\Delta f D/c_0}}{(R_{t2}^2-R_{t1}^2)(R_{r2}^2-R_{r1}^2)}. \quad (34)$$

To obtain the STF-CFs for the 3-D reference model, the integrals in (22)–(24) must numerically be evaluated, because they do not have closed-form solutions.

B. sD-psd

The sD-psd of the time-variant transfer function is the Fourier transform of the space–time correlation function $R_{pq,\tilde{p}\tilde{q}}(\Delta t,\Delta f=0)$. From (21), it follows that the sD-psd is a summation of the sD-psd functions of the single-bounced transmit, single-bounced receive, double-bounced, and LoS components. In [9], it is shown that the sD-psds of the single-bounced transmit, single-bounced receive, double-bounced, and LoS components are, respectively

$$S_{pq,\tilde{p}\tilde{q}}^{SBT}(\nu) = \mathcal{F}_{\Delta t}\left\{R_{pq,\tilde{p}\tilde{q}}^{SBT}(\Delta t,\Delta f=0)\right\} = \frac{\eta_T}{I_0(k_T)} \frac{\cos\left(\frac{2\pi}{\lambda}\beta_{T_m}(p-\tilde{p})d_{Tz}\right)}{1-\left(\frac{4\beta_{T_m}(p-\tilde{p})d_{Tz}}{\lambda}\right)^2} \times \frac{(3-2\gamma R_{t2}/D)R_{t2}^2-(3-2\gamma R_{t1}/D)R_{t1}^2}{3\left(R_{t2}^2-R_{t1}^2\right)} \times \frac{\exp\left\{j2\pi(\nu+f_{R\max}\cos\gamma_R)A_{SBT}-j2\pi p_{x_{SBR}}\right\}}{\pi f_{T\max}\sqrt{1-\left[(\nu+f_{R\max}\cos\gamma_R)/f_{T\max}\right]^2}} \times \cosh\Bigg[(k_T\sin(\mu_T-\gamma_T)+j2\pi p_{x_{SBT}}q_{y_{SBT}} - j2\pi p_{y_{SBT}}q_{x_{SBT}})\sqrt{1-\left[(\nu+f_{R\max}\cos\gamma_R)/f_{T\max}\right]^2}\Bigg] \quad (35)$$

$$S_{pq,\tilde{p}\tilde{q}}^{SBR}(\nu) = \mathcal{F}_{\Delta t}\{R_{pq,\tilde{p}\tilde{q}}^{SBR}(\Delta t,\Delta f=0)\} = \frac{\eta_R}{I_0(k_R)} \frac{\cos\left(\frac{2\pi}{\lambda}\beta_{R_m}(q-\tilde{q})d_{Rz}\right)}{1-\left(\frac{4\beta_{R_m}(q-\tilde{q})d_{Rz}}{\lambda}\right)^2} \times \frac{\exp\left\{j2\pi(\nu-f_{T\max}\cos\gamma_T)A_{SBR}+j2\pi p_{x_{SBT}}\right\}}{\pi f_{R\max}\sqrt{1-\left[(\nu-f_{T\max}\cos\gamma_T)/f_{R\max}\right]^2}} \times \frac{(3-2\gamma R_{r2}/D)R_{r2}^2-(3-2\gamma R_{r1}/D)R_{r1}^2}{3\left(R_{r2}^2-R_{r1}^2\right)} \times \cosh\Bigg[(k_R\sin(\mu_R-\gamma_R)+j2\pi p_{x_{SBR}}q_{y_{SBR}} - j2\pi p_{y_{SBR}}q_{x_{SBR}})\sqrt{1-\left[(\nu-f_{T\max}\cos\gamma_T)/f_{R\max}\right]^2}\Bigg] \quad (36)$$

$$S_{pq,\tilde{p}\tilde{q}}^{DB}(\nu) = \mathcal{F}_{\Delta t}\{R_{pq,\tilde{p}\tilde{q}}^{DB}(\Delta t,\Delta f=0)\}$$

$$= \frac{\eta_{TR} I_{DB}}{I_0(k_T) I_0(k_R)}$$
$$\times \frac{\cos\left(\frac{2\pi}{\lambda}\beta_{T_m}(p-\tilde{p})d_{Tz}\right)}{1-\left(\frac{4\beta_{T_m}(p-\tilde{p})d_{Tz}}{\lambda}\right)^2} \frac{\cos\left(\frac{2\pi}{\lambda}\beta_{R_m}(q-\tilde{q})d_{Rz}\right)}{1-\left(\frac{4\beta_{R_m}(q-\tilde{q})d_{Rz}}{\lambda}\right)^2}$$
$$\times e^{j(2\pi p_{x_{DB}} q_{x_{DB}} + 2\pi p_{y_{DB}} q_{y_{DB}} - jk_T \cos(\mu_T - \gamma_T))\nu / f_{T\max}}$$
$$\times \frac{1}{\pi f_{T\max}\sqrt{1-(\nu/f_{T\max})^2}} \cosh\Bigg[(k_T \sin(\mu_T - \gamma_T)$$
$$+ j2\pi p_{x_{DB}} q_{y_{DB}} - j2\pi p_{y_{DB}} q_{x_{DB}}) \sqrt{1-(\nu/f_{T\max})^2}\Bigg]$$
$$\odot e^{j(2\pi p_{z_{DB}} q_{z_{DB}} + 2\pi p_{w_{DB}} q_{w_{DB}} - jk_R \cos(\mu_R - \gamma_R))\nu / f_{R\max}}$$
$$\times \frac{1}{\pi f_{R\max}\sqrt{1-(\nu/f_{R\max})^2}} \cosh\Bigg[(k_R \sin(\mu_R - \gamma_R)$$
$$+ j2\pi p_{z_{DB}} q_{w_{DB}} - j2\pi p_{w_{DB}} q_{z_{DB}}) \sqrt{1-(\nu/f_{R\max})^2}\Bigg] \quad (37)$$

$$S^{LoS}_{pq,\tilde{p}\tilde{q}}(\nu) = \mathcal{F}_{\Delta t}\left\{R^{LoS}_{pq,\tilde{p}\tilde{q}}(\Delta t, \Delta f = 0)\right\} = K e^{j\frac{2\pi}{\lambda}(p-\tilde{p})d_{Tx}}$$
$$\times e^{-j\frac{2\pi}{\lambda}(q-\tilde{q})d_{Rx}} \delta(\nu + f_{T\max}\cos\gamma_T - f_{R\max}\cos\gamma_R) \quad (38)$$

where $\mathcal{F}\{\cdot\}$ denotes the Fourier transform, $\cosh(\cdot)$ is the hyperbolic cosine, $\delta(\cdot)$ is the Dirac delta function, $|\nu + f_{R\max}\cos\gamma_R| \le f_{T\max}$ and $|\nu - f_{T\max}\cos\gamma_T| \le f_{R\max}$ for the single-bounced sD-psds, and $|\nu| \le f_{T\max} + f_{R\max}$ for the double-bounced sD-psd. Finally, the parameters in (35)–(37) are defined as follows: $A_{SBT} = (2\pi p_{x_{SBT}} q_{x_{SBT}} + 2\pi p_{y_{SBT}} q_{y_{SBT}} - w_{x_{SBT}})/2\pi f_{T\max}$, $p_{x_{SBT}} = (p-\tilde{p})d_{Tx}/\lambda$, $q_{x_{SBT}} = \cos\gamma_T$, $w_{x_{SBT}} = jk_T\cos(\gamma_T - \mu_T)$, $p_{y_{SBT}} = [(p-\tilde{p})d_{Ty} + (q-\tilde{q})d_{Ry}(R_{t1} + 0.5(R_{t2} - R_{t1}))/D]/\lambda$, $q_{y_{SBT}} = \sin\gamma_T$, $w_{y_{SBT}} = jk_T\sin(\gamma_T - \mu_T)$, $q_{x_{SBR}} = \cos\gamma_R$, $p_{x_{SBR}} = (q-\tilde{q})d_{Rx}/\lambda$, $A_{SBR} = (2\pi p_{x_{SBR}} q_{x_{SBR}} + 2\pi p_{y_{SBR}} q_{y_{SBR}} + w_{x_{SBR}})/2\pi f_{R\max}$, $w_{x_{SBR}} = -jk_R\cos(\gamma_R - \mu_R)$, $p_{y_{SBR}} = [(q-\tilde{q})d_{Ry} + (p-\tilde{p})d_{Ty}(R_{r1} + 0.5(R_{r2} - R_{r1}))/D]/\lambda$, $q_{y_{SBR}} = \sin\gamma_R$, and $w_{y_{SBR}} = -jk_R\sin(\gamma_R - \mu_R)$, $p_{x_{DB}} = (p-\tilde{p})d_{Tx}/\lambda$, $q_{x_{DB}} = \cos\gamma_T$, $p_{y_{DB}} = (p-\tilde{p})d_{Ty}/\lambda$, $q_{y_{DB}} = \sin\gamma_T$, $p_{z_{DB}} = (q-\tilde{q})d_{Rx}/\lambda$, $q_{z_{DB}} = \cos\gamma_R$, $p_{w_{DB}} = (q-\tilde{q})d_{Ry}/\lambda$, $q_{w_{DB}} = \sin\gamma_R$, and $I_{DB} = (R^2_{t2} - R^2_{t1}) \times (0.5R^2_{r2} - \gamma R^3_{r2}/(3D) - 0.5R^2_{r1} + \gamma R^3_{r1}/(3D)) + (R^2_{r2} - R^2_{r1})(0.5R^2_{t2} - \gamma R^3_{t2}/(3D) - 0.5R^2_{t1} + \gamma R^3_{t1}/(3D))$.

C. PSDS

The psds of the time-variant transfer function is the inverse Fourier transform of the space–frequency correlation function $R_{pq,\tilde{p}\tilde{q}}(\Delta t = 0, \Delta f)$. From (21), it follows that the psds is a summation of the psds functions of the single-bounced transmit, single-bounced receive, double-bounced, and LoS components. In [11], it is shown that the psds of the single-bounced transmit, single-bounced receive, double-bounced, and LoS components are, respectively

$$P^{SBT}_{pq,\tilde{p}\tilde{q}}(\tau_{\rm rel}) = \mathcal{F}^{-1}_{\Delta f}\left\{R^{SBT}_{pq,\tilde{p}\tilde{q}}(\Delta t = 0, \Delta f)\right\} = \frac{\eta_T}{I_0(k_T)}$$
$$\times \frac{\cos\left(\frac{2\pi}{\lambda}\beta_{T_m}(p-\tilde{p})d_{Tz}\right)}{1-\left(\frac{4\beta_{T_m}(p-\tilde{p})d_{Tz}}{\lambda}\right)^2} e^{-j\frac{2\pi}{\lambda}(q-\tilde{q})d_{Rx}} \frac{2}{R^2_{t2} - R^2_{t1}}$$
$$\times \int_{R_{ta}}^{R_{tb}} \left(1 - \frac{\gamma R_t}{D}\right) R_t e^{j\frac{2\pi}{c_0}R_t B_{SBT}(c_0\tau_{\rm rel}/R_t - 1)}$$
$$\times \frac{\cosh\left(2jC_{SBT}\sqrt{\frac{c_0\tau_{\rm rel}}{2R_t}\left(1 - \frac{c_0\tau_{\rm rel}}{2R_t}\right)}\right)}{\frac{2\pi}{c_0}R_t\sqrt{\frac{c_0\tau_{\rm rel}}{2R_t}\left(1 - \frac{c_0\tau_{\rm rel}}{2R_t}\right)}} dR_t \quad (39)$$

$$P^{SBR}_{pq,\tilde{p}\tilde{q}}(\tau_{\rm rel}) = \mathcal{F}^{-1}_{\Delta f}\left\{R^{SBR}_{pq,\tilde{p}\tilde{q}}(\Delta t = 0, \Delta f)\right\} = \frac{\eta_R}{I_0(k_R)}$$
$$\times \frac{\cos\left(\frac{2\pi}{\lambda}\beta_{R_m}(q-\tilde{q})d_{Rz}\right)}{1-\left(\frac{4\beta_{R_m}(q-\tilde{q})d_{Rz}}{\lambda}\right)^2} e^{j\frac{2\pi}{\lambda}(p-\tilde{p})d_{Tx}} \frac{2}{R^2_{r2} - R^2_{r1}}$$
$$\times \int_{R_{ra}}^{R_{rb}} \left(1 - \gamma\frac{R_r}{D}\right) R_r e^{j\frac{2\pi}{c_0}R_r B_{SBR}(c_0\tau_{\rm rel}/R_r - 1)}$$
$$\times \frac{\cosh\left(2jC_{SBR}\sqrt{\frac{c_0\tau_{\rm rel}}{2R_r}\left(1 - \frac{c_0\tau_{\rm rel}}{2R_r}\right)}\right)}{\frac{2\pi}{c_0}R_r\sqrt{\frac{c_0\tau_{\rm rel}}{2R_r}\left(1 - \frac{c_0\tau_{\rm rel}}{2R_r}\right)}} dR_r \quad (40)$$

$$P^{DB}_{pq,\tilde{p}\tilde{q}}(\tau_{\rm rel}) = \mathcal{F}^{-1}_{\Delta f}\left\{R^{DB}_{pq,\tilde{p}\tilde{q}}(\Delta t = 0, \Delta f)\right\} = \frac{\eta_{TR}}{I_0(k_T)I_0(k_R)}$$
$$\times \frac{\cos\left(\frac{2\pi}{\lambda}\beta_{T_m}(p-\tilde{p})d_{Tz}\right)}{1-\left(\frac{4\beta_{T_m}(p-\tilde{p})d_{Tz}}{\lambda}\right)^2} \frac{\cos\left(\frac{2\pi}{\lambda}\beta_{R_m}(q-\tilde{q})d_{Rz}\right)}{1-\left(\frac{4\beta_{R_m}(q-\tilde{q})d_{Rz}}{\lambda}\right)^2}$$
$$\times \frac{2}{(R^2_{t2} - R^2_{t1})(R^2_{r2} - R^2_{r1})} \Bigg[\int_{R_{ta}}^{R_{tb}} R_t e^{j\frac{2\pi}{c_0}R_t B_{DB}\left(\frac{c_0\tau_{\rm rel}}{R_t} - 1\right)}$$
$$\times \frac{\cosh\left(2jC_{DB}\sqrt{\frac{c_0\tau_{\rm rel}}{2R_t}\left(1 - \frac{c_0\tau_{\rm rel}}{2R_t}\right)}\right)}{\frac{2\pi}{c_0}R_t\sqrt{\frac{c_0\tau_{\rm rel}}{2R_t}\left(1 - \frac{c_0\tau_{\rm rel}}{2R_t}\right)}} dR_t \odot \int_{R_{ra}}^{R_{rb}} \left(1 - \gamma\frac{R_r}{D}\right) R_r$$
$$\times \frac{e^{j\frac{2\pi}{c_0}R_r D_{DB}\left(\frac{c_0\tau_{\rm rel}}{R_r} - 1\right)} \cosh\left(2jE_{DB}\sqrt{\frac{c_0\tau_{\rm rel}}{2R_r}\left(1 - \frac{c_0\tau_{\rm rel}}{2R_r}\right)}\right)}{\frac{2\pi}{c_0}R_r\sqrt{\frac{c_0\tau_{\rm rel}}{2R_r}\left(1 - \frac{c_0\tau_{\rm rel}}{2R_r}\right)}} dR_r$$
$$+ \int_{R_{ta}}^{R_{tb}} \left(1 - \gamma\frac{R_t}{D}\right) R_t \frac{\cosh\left(2jC_{DB}\sqrt{\frac{c_0\tau_{\rm rel}}{2R_t}\left(1 - \frac{c_0\tau_{\rm rel}}{2R_t}\right)}\right)}{\frac{2\pi}{c_0}R_t\sqrt{\frac{c_0\tau_{\rm rel}}{2R_t}\left(1 - \frac{c_0\tau_{\rm rel}}{2R_t}\right)}}$$
$$\times e^{j\frac{2\pi}{c_0}R_t B_{DB}\left(\frac{c_0\tau_{\rm rel}}{R_t} - 1\right)} dR_t \odot \int_{R_{ra}}^{R_{rb}} R_r e^{j\frac{2\pi}{c_0}R_r D_{DB}\left(\frac{c_0\tau_{\rm rel}}{R_r} - 1\right)}$$
$$\times \frac{\cosh\left(2jE_{DB}\sqrt{\frac{c_0\tau_{\rm rel}}{2R_r}\left(1 - \frac{c_0\tau_{\rm rel}}{2R_r}\right)}\right)}{\frac{2\pi}{c_0}R_r\sqrt{\frac{c_0\tau_{\rm rel}}{2R_r}\left(1 - \frac{c_0\tau_{\rm rel}}{2R_r}\right)}} dR_r \Bigg] \quad (41)$$

$$P^{LoS}_{pq,\tilde{p}\tilde{q}}(\tau_{\rm rel}) = \mathcal{F}^{-1}_{\Delta f}\left\{R^{LoS}_{pq,\tilde{p}\tilde{q}}(\Delta t = 0, \Delta f)\right\}$$
$$= K e^{j\frac{2\pi}{\lambda}[(p-\tilde{p})d_{Tx} - (q-\tilde{q})d_{Rx}]} \delta\left(\tau - \frac{\sqrt{D^2 + \Delta^2_H}}{c_0}\right) \quad (42)$$

where $\cosh(\cdot)$ is the hyperbolic cosine, $\odot$ denotes convolution, $\delta(\cdot)$ denotes the Dirac delta function, and $\tau_{\rm rel} = \tau - D/c_0$. The integrals in (39)–(41) need to be numerically evaluated

over the range of possible radii R_t and R_r. For the range $0 \le \tau_{\rm rel} \le 2R_{t1}/c_0$, the integration limits are $R_{ta} = R_{t1}$, $R_{tb} = R_{t2}$, $R_{ra} = R_{r1}$, and $R_{rb} = R_{r2}$. On the other hand, when $2R_{t1}/c_0 \le \tau_{\rm rel} \le 2R_{t2}/c_0$, the integration limits are $R_{ta} = c_0\tau_{\rm rel}/2$, $R_{tb} = R_{t2}$, $R_{ra} = c_0\tau_{\rm rel}/2$, and $R_{rb} = R_{r2}$. Finally, the parameters in (39)–(41) are defined as follows: $B_{SBT} = (2\pi(p-\tilde{p})d_{Tx}/\lambda - jk_T\cos\mu_T)/\pi\tau_t$, $C_{SBT} = (2\pi(p-\tilde{p})d_{Ty}/\lambda + 2\pi(q-\tilde{q})d_{Ry}(R_{t1}+\ 0.5(R_{t2}-R_{t1}))/D\lambda - jk_T\sin\mu_T)$, $\tau_t = 2R_t/c_0$, $B_{SBR} = (2\pi(q-\tilde{q})d_{Rx}/\lambda - jk_R\cos\mu_R)/\pi\tau_r$, $C_{SBR} = (2\pi(q-\tilde{q})d_{Ry}/\lambda + 2\pi(q-\tilde{q})d_{Ty}(R_{r1}+\ 0.5(R_{r2}-R_{r1}))/D\lambda - jk_R\sin\mu_R)$, $\tau_r = 2R_r/c_0$, $B_{DB} = (2\pi(p-\tilde{p})d_{Tx}/\lambda - jk_T\cos\mu_T)/\pi\tau_t$, $C_{DB} = 2\pi(p-\tilde{p})d_{Ty}/\lambda - jk_T\sin\mu_T$, $D_{DB} = (2\pi(q-\tilde{q})d_{Rx}/\lambda - jk_R\cos\mu_R)/\pi\tau_r$, $E_{DB} = 2\pi(q-\tilde{q})d_{Ry}/\lambda - jk_R\sin\mu_R$, and $\tau_{\rm rel} = \tau - D/c_0$.

D. LCR

The LCR $L(R)$ is defined as the rate at which the signal envelope crosses the level R in the positive (or negative) direction. When a LoS component is present, the LCR can be written as [23]

$$L(R) = \frac{2R\sqrt{K+1}}{\pi^{3/2}}\sqrt{\frac{b_2}{b_0}-\frac{b_1^2}{b_0^2}}e^{-K-(K+1)R^2} \times \int_0^{\pi/2}\cosh\left(2\sqrt{K(K+1)}R\cos\theta\right) \times \left[e^{-(\chi\sin\theta)^2}+\sqrt{\pi}\chi\sin\theta\,\mathrm{erf}(\chi\sin\theta)\right]d\theta \quad (43)$$

where $\cosh(\cdot)$ is the hyperbolic cosine function, $\mathrm{erf}(\cdot)$ is the error function, and the parameter χ is equal to $\sqrt{Kb_1^2/(b_0b_2-b_1^2)}$. Finally, the parameters b_0, b_1, and b_2 can be written as [11]

$$b_n = b_n^{SBT} + b_n^{SBR} + b_n^{DB} \quad (44)$$

where $n \in \{0,1,2\}$, and the parameters b_0^{DB}, b_0^{SBT}, b_0^{SBR}, b_1^{DB}, b_1^{SBT}, b_1^{SBR}, b_2^{DB}, b_2^{SBT}, and b_2^{SBR} are, respectively, $2b_0^{DB} = \eta_{TR}/(K+1)$, $2b_0^{SBT} = \eta_T/(K+1)$, and $2b_0^{SBR} = \eta_R/(K+1)$

$$b_1^{DB} = 2\pi b_0^{DB}\left\{f_{T\max}\cos(\mu_T-\gamma_T)\frac{I_1(k_T)}{I_0(k_T)}\frac{\pi^2\cos\beta_{T_m}}{\pi^2-4\beta_{T_m}^2} + f_{R\max}\cos(\mu_R-\gamma_R)\frac{I_1(k_R)}{I_0(k_R)}\frac{\pi^2\cos\beta_{R_m}}{\pi^2-4\beta_{R_m}^2}\right\} \quad (45)$$

$$b_1^{SBT} = 2\pi b_0^{SBT}\left\{f_{T\max}\cos(\mu_T-\gamma_T)\frac{I_1(k_T)}{I_0(k_T)}\frac{\pi^2\cos\beta_{T_m}}{\pi^2-4\beta_{T_m}^2} + \int_{R_{t1}}^{R_{t2}}\left[\frac{R_t}{D}\sin\gamma_R\sin\mu_T\frac{I_1(k_T)}{I_0(k_T)}+\cos\gamma_R\right] \times f_{R\max}\frac{2R_t}{R_{t2}^2-R_{t1}^2} \times \frac{\pi^2\left[\cos\left(\frac{R_t}{D}\beta_{T_m}+\frac{\Delta_H}{D}\right)+\cos\left(\frac{R_t}{D}\beta_{T_m}-\frac{\Delta_H}{D}\right)\right]}{2\left[\pi^2-4\left(\frac{R_t}{D}\right)^2\beta_{T_m}^2\right]}dR_t\right\} \quad (46)$$

$$b_1^{SBR} = 2\pi b_0^{SBR}\left\{f_{R\max}\cos(\mu_R-\gamma_R)\frac{I_1(k_R)}{I_0(k_R)}\frac{\pi^2\cos\beta_{R_m}}{\pi^2-4\beta_{R_m}^2} - \int_{R_{r1}}^{R_{r2}}\left[\frac{R_r}{D}\sin\gamma_T\sin\mu_R\frac{I_1(k_R)}{I_0(k_R)}-\cos\gamma_T\right]f_{T\max}\frac{2R_r}{R_{r2}^2-R_{r1}^2} \times \frac{\pi^2\left[\cos\left(\frac{R_r}{D}\beta_{R_m}+\frac{\Delta_H}{D}\right)+\cos\left(\frac{R_r}{D}\beta_{R_m}-\frac{\Delta_H}{D}\right)\right]}{2\left[\pi^2-4\left(\frac{R_r}{D}\right)^2\beta_{R_m}^2\right]}dR_r\right\} \quad (47)$$

$$b_2^{DB} = (2\pi)^2 b_0^{DB}\left\{f_{T\max}^2\left[\frac{\pi^2\cos(2\beta_{T_m})}{2\left(\pi^2-16\beta_{T_m}^2\right)}+\frac{1}{2}\right] \times \frac{1+\cos\left(2(\mu_T-\gamma_T)\right)I_2(k_T)}{2I_0(k_T)} + 2f_{T\max}f_{R\max}\frac{\pi^2\cos\beta_{T_m}}{\pi^2-4\beta_{T_m}^2} \times \frac{\pi^2\cos\beta_{R_m}}{\pi^2-4\beta_{R_m}^2}\cos(\mu_T-\gamma_T)\frac{I_1(k_T)}{I_0(k_T)}\cos(\mu_R-\gamma_R)\frac{I_1(k_R)}{I_0(k_R)} + f_{R\max}^2\left[\frac{\pi^2\cos(2\beta_{R_m})}{2\left(\pi^2-16\beta_{R_m}^2\right)}+\frac{1}{2}\right]\frac{1+\cos(2(\mu_R-\gamma_R))I_2(k_R)}{2I_0(k_R)}\right\} \quad (48)$$

$$b_2^{SBT} = (2\pi)^2 b_0^{SBT}\left\{f_{T\max}^2\frac{\pi^2\cos(2\beta_{T_m})+\pi^2-16\beta_{T_m}^2}{2\left(\pi^2-16\beta_{T_m}^2\right)} \times \frac{1+\cos\left(2(\mu_T-\gamma_T)\right)I_2(k_T)}{2I_0(k_T)} + \int_{R_{t1}}^{R_{t2}}\frac{4\beta_{T_m}^2+8\frac{R_t}{D}\beta_{T_m}^2-\pi^2+4\left(\frac{R_t}{D}\right)^2\beta_{T_m}^2}{4F_{SBT}} \times \left[\cos\left(\left(\frac{R_t}{D}-1\right)\beta_{T_m}+\frac{\Delta_H}{D}\right)+\cos\left(\left(\frac{R_t}{D}+1\right)\beta_{T_m}+\frac{\Delta_H}{D}\right) + \cos\left(\left(\frac{R_t}{D}-1\right)\beta_{T_m}-\frac{\Delta_H}{D}\right)+\cos\left(\left(\frac{R_t}{D}+1\right)\beta_{T_m}-\frac{\Delta_H}{D}\right)\right] \times \left[f_{T\max}f_{R\max}\frac{R_t}{D}\sin\gamma_R\left(\frac{I_2(k_T)}{I_0(k_T)}\cos(2\mu_T-\gamma_T) - \cos\gamma_T\right)+2f_{T\max}f_{R\max}\cos\gamma_R\right] + \left[\frac{\cos\left[2\left(\frac{R_t}{D}\beta_{T_m}+\frac{\Delta_H}{D}\right)\right]\pi^2+2\pi^2-32\left(\frac{R_t}{D}\right)^2\beta_{T_m}^2}{4\left[\pi^2-16\left(\frac{R_t}{D}\right)^2\beta_{T_m}\right]} + \frac{\cos\left[2\left(\frac{R_t}{D}\beta_{T_m}-\frac{\Delta_H}{D}\right)\right]\pi^2}{4\left[\pi^2-16\left(\frac{R_t}{D}\right)^2\beta_{T_m}\right]}\right]\left[f_{R\max}^2\cos\gamma_R^2 + f_{R\max}^2\left(\frac{R_t}{D}\right)^2\sin\gamma_R^2\frac{1-\cos(2\mu_T)I_2(k_T)}{2I_0(k_T)} + f_{R\max}^2\frac{R_t}{D}\sin(2\gamma_R)\sin\mu_T\frac{I_1(k_T)}{I_0(k_T)}\right]\frac{2R_t}{R_{t2}^2-R_{t1}^2}dR_t\right\} \quad (49)$$

$$b_2^{SBR} = (2\pi)^2 b_0^{SBR} \Bigg\{ f_{R\max}^2 \frac{\pi^2\cos(2\beta_{R_m})+\pi^2-16\beta_{R_m}^2}{2\left(\pi^2-16\beta_{R_m}^2\right)} \times \frac{1+\cos\left(2(\mu_R-\gamma_R)\right) I_2(k_R)}{2I_0(k_R)} + \int_{R_{r1}}^{R_{r2}} \frac{4\beta_{R_m}^2+8\frac{R_r}{D}\beta_{R_m}^2-\pi^2+4\left(\frac{R_r}{D}\right)^2\beta_{R_m}^2}{4F_{SBR}} \times \left[\cos\left(\left(\frac{R_r}{D}-1\right)\beta_{R_m}+\frac{\Delta_H}{D}\right)+\cos\left(\left(\frac{R_r}{D}+1\right)\beta_{R_m}+\frac{\Delta_H}{D}\right) + \cos\left(\left(\frac{R_r}{D}-1\right)\beta_{R_m}-\frac{\Delta_H}{D}\right)+\cos\left(\left(\frac{R_r}{D}+1\right)\beta_{R_m}-\frac{\Delta_H}{D}\right)\right] \times \left[f_{R\max}f_{T\max}\frac{R_r}{D}\sin\gamma_T\left(\cos\gamma_R - \frac{I_2(k_R)}{I_0(k_R)}\cos(2\mu_R-\gamma_R)\right)+2f_{R\max}f_{T\max}\cos\gamma_T\right] + \left[\frac{\cos\left[2\left(\frac{R_r}{D}\beta_{R_m}+\frac{\Delta_H}{D}\right)\right]\pi^2+2\pi^2-32\left(\frac{R_r}{D}\right)^2\beta_{R_m}^2}{4\left[\pi^2-16\left(\frac{R_r}{D}\right)^2\beta_{R_m}\right]} + \frac{\cos\left[2\left(\frac{R_r}{D}\beta_{R_m}-\frac{\Delta_H}{D}\right)\right]\pi^2}{4\left[\pi^2-16\left(\frac{R_r}{D}\right)^2\beta_{R_m}\right]}\right]\left[f_{T\max}^2\cos\gamma_T^2 + f_{T\max}^2\left(\frac{R_r}{D}\right)^2\sin\gamma_T^2\frac{1-\cos(2\mu_R)I_2(k_R)}{2I_0(k_R)} - f_{T\max}^2\frac{R_r}{D}\sin(2\gamma_T)\sin\mu_R\frac{I_1(k_R)}{I_0(k_R)}\right]\frac{2R_r}{R_{r2}^2-R_{r1}^2}dR_r\Bigg\}. \quad (50)$$

In addition, $F_{SBT} = 8\beta_{T_m}^2\pi^2 - 16\beta_{T_m}^4 - \pi^4 - 16(R_t/D)^4\beta_{T_m}^4 + 8\pi^2(R_t/D)^2\beta_{T_m}^2 + 32(R_t/D)^2\beta_{T_m}^4$, and $F_{SBR} = 8\beta_{R_m}^2\pi^2 - 16\beta_{R_m}^4 - \pi^4 - 16(R_r/D)^4\beta_{R_m}^4 + 8\pi^2(R_r/D)^2\beta_{R_m}^2 + 32(R_r/D)^2\beta_{R_m}^4$.

APPENDIX B
CRLB

This section derives the CRLB for the estimator in Section IV. The CRLB for each element of the vector $\mathbf{\Theta} = [\Theta_i]_{i=1}^8 = [\beta_{T_m}, k_T, \mu_T, \beta_{R_m}, k_R, \mu_R, \eta_T, \eta_R]$ can be obtained from the inverse Fisher information matrix. The (i,j)th element of the Fisher information matrix can be written as $[\mathbf{F}(\mathbf{\Theta})]_{i,j} = -\mathrm{E}[\partial^2\mathcal{L}(\mathbf{\Theta})/\partial\Theta_i\partial\Theta_j]$, where $i, j \in \{1,\ldots,8\}$. To obtain the elements of the Fisher information matrix, we calculate the first and the second derivative of the log-likelihood function in (17) as follows:

$$\frac{\partial\mathcal{L}(\mathbf{\Theta}_{T,F})}{\partial\Theta_i} = -N_s\frac{\partial\left(\mathrm{tr}\left\{\mathbf{R}(\mathbf{\Theta}_{T,F},T\Delta t_s,F\Delta f_s)^{-1}\hat{\mathbf{R}}(T\Delta t_s,F\Delta f_s)\right\}\right)}{\partial\Theta_i} - N_s\frac{\partial\left(\ln|\mathbf{R}(\mathbf{\Theta}_{T,F},T\Delta t_s,F\Delta f_s)|\right)}{\partial\Theta_i} = -N_s \times \mathrm{tr}\Big[\Big[\mathbf{I}_{L_TL_R} - \mathbf{R}(\mathbf{\Theta}_{T,F},T\Delta t_s,F\Delta f_s)^{-1}\hat{\mathbf{R}}(T\Delta t_s,F\Delta f_s)\Big] \times \mathbf{R}(\mathbf{\Theta}_{T,F},T\Delta t_s,F\Delta f_s)^{-1}\mathbf{D}_{\Theta_i}(\mathbf{\Theta}_{T,F},T\Delta t_s,F\Delta f_s)\Big] \quad (51)$$

$$\frac{\partial^2\mathcal{L}(\mathbf{\Theta}_{T,F})}{\partial\Theta_i\partial\Theta_j} = -N_s\mathrm{tr}\Bigg\{\frac{\partial}{\partial\Theta_j} \times \Big[\Big(\mathbf{I}_{L_TL_R} - \mathbf{R}(\mathbf{\Theta}_{T,F},T\Delta t_s,F\Delta f_s)^{-1}\hat{\mathbf{R}}(T\Delta t_s,F\Delta f_s)\Big) \times \mathbf{R}(\mathbf{\Theta}_{T,F},T\Delta t_s,F\Delta f_s)^{-1}\mathbf{D}_{\Theta_i}(\mathbf{\Theta}_{T,F},T\Delta t_s,F\Delta f_s)\Big] + \Big(\mathbf{I}_{L_TL_R} - \mathbf{R}(\mathbf{\Theta}_{T,F},T\Delta t_s,F\Delta f_s)^{-1}\hat{\mathbf{R}}(T\Delta t_s,F\Delta f_s)\Big) \times \frac{\partial}{\partial\Theta_j}\left[\mathbf{R}(\mathbf{\Theta}_{T,F},T\Delta t_s,F\Delta f_s)^{-1} \times \mathbf{D}_{\Theta_i}(\mathbf{\Theta}_{T,F},T\Delta t_s,F\Delta f_s)\right]\Bigg\} = -N_s \times \mathrm{tr}\Bigg\{\mathbf{R}(\mathbf{\Theta}_{T,F},T\Delta t_s,F\Delta f_s)^{-1}\mathbf{D}_{\Theta_j}(\mathbf{\Theta}_{T,F},T\Delta t_s,F\Delta f_s) \times \mathbf{R}(\mathbf{\Theta}_{T,F},T\Delta t_s,F\Delta f_s)^{-1}\hat{\mathbf{R}}(T\Delta t_s,F\Delta f_s) \times \mathbf{R}(\mathbf{\Theta}_{T,F},T\Delta t_s,F\Delta f_s)^{-1}\mathbf{D}_{\Theta_i}(\mathbf{\Theta}_{T,F},T\Delta t_s,F\Delta f_s) + \Big(\mathbf{I}_{L_TL_R} - \mathbf{R}(\mathbf{\Theta}_{T,F},T\Delta t_s,F\Delta f_s)^{-1}\hat{\mathbf{R}}(T\Delta t_s,F\Delta f_s)\Big)\frac{\partial}{\partial\Theta_j} \times \Big[\mathbf{R}(\mathbf{\Theta}_{T,F},T\Delta t_s,F\Delta f_s)^{-1}\mathbf{D}_{\Theta_i}(\mathbf{\Theta}_{T,F},T\Delta t_s,F\Delta f_s)\Big]\Bigg\} \quad (52)$$

where $\mathbf{D}_{\Theta_i}(\mathbf{\Theta}_{T,F},T\Delta t_s,F\Delta f_s) = \partial\mathbf{R}(\mathbf{\Theta}_{T,F},T\Delta t_s,F\Delta f_s)/\partial\Theta_i$, $\mathbf{I}_{L_tL_r}$ is the $L_tL_r \times L_tL_r$ identity matrix, and $\mathbf{D}_{\Theta_j}(\mathbf{\Theta}_{T,F},T\Delta t_s,F\Delta f_s) = \partial\mathbf{R}(\mathbf{\Theta}_{T,F},T\Delta t_s,F\Delta f_s)/\partial\Theta_j$.

By observing that $\mathrm{E}[\hat{\mathbf{R}}(T\Delta t_s,F\Delta f_s)] = \mathbf{R}(\mathbf{\Theta}_{T,F},T\Delta t_s, F\Delta f_s)$, the (i,j)th element of the Fisher information matrix becomes

$$[\mathbf{F}(\mathbf{\Theta})]_{i,j} = -\mathrm{E}\left[\frac{\partial^2\mathcal{L}(\mathbf{\Theta})}{\partial\Theta_i\partial\Theta_j}\right] = \frac{N_s}{t_{\max}f_{\max}}\sum_{T=0}^{t_{\max}-1}\sum_{F=0}^{f_{\max}-1} \times \mathrm{tr}\big\{\mathbf{R}(\mathbf{\Theta}_{T,F},T\Delta t_s,F\Delta f_s)^{-1}\mathbf{D}_{\Theta_j}(\mathbf{\Theta}_{T,F},T\Delta t_s,F\Delta f_s) \times \mathbf{R}(\mathbf{\Theta}_{T,F},T\Delta t_s,F\Delta f_s)^{-1}\mathbf{D}_{\Theta_i}(\mathbf{\Theta}_{T,F},T\Delta t_s,F\Delta f_s)\big\} \quad (53)$$

where the derivatives $\mathbf{D}_{\Theta_i}(\mathbf{\Theta}_{T,F},T\Delta t_s,F\Delta f_s)$ for $i \in \{1,\ldots,8\}$ are given by

$$[\mathbf{D}_{\Theta_1}(\mathbf{\Theta}_{T,F},T\Delta t_s,F\Delta f_s)]_{q+L_r(p-1),\tilde{q}+L_r(\tilde{p}-1)} = \left[\frac{\partial\mathbf{R}(\mathbf{\Theta}_{T,F},T\Delta t_s,F\Delta f_s)}{\partial\beta_{T_m}}\right]_{q+L_r(p-1),\tilde{q}+L_r(\tilde{p}-1)} = \frac{\partial R_{pq,\tilde{p}\tilde{q}}^{SBT}(T\Delta t_s,F\Delta f_s)}{\partial\beta_{T_m}} + \frac{\partial R_{pq,\tilde{p}\tilde{q}}^{DB}(T\Delta t_s,F\Delta f_s)}{\partial\beta_{T_m}}$$

$$
\begin{aligned}
&= \left\{ \frac{\eta_T}{I_0(k_T)} e^{-j\frac{2\pi}{\lambda}(q-\tilde{q})d_{Rx}} e^{-j2\pi T\Delta t_s f_{R\max}\cos\gamma_R} \right.\\
&\times \int_{R_{t1}}^{R_{t2}} \left(1-\gamma\frac{R_t}{D}\right) e^{-j\frac{2\pi}{c_0}F\Delta f_s(D+R_t)} I_0\left(\sqrt{x_{SBT}^2+y_{SBT}^2}\right)\\
&\times \frac{2R_t dR_t}{R_{t2}^2-R_{t1}^2} + \left[\int_{R_{t1}}^{R_{t2}} 2e^{-j\frac{2\pi}{c_0}F\Delta f_s R_t} R_t I_0\left(\sqrt{x_{DB}^2+y_{DB}^2}\right) dR_t \right.\\
&\times \int_{R_{r1}}^{R_{r2}} e^{-j\frac{2\pi}{c_0}F\Delta f_s R_r} R_r I_0\left(\sqrt{w_{DB}^2+z_{DB}^2}\right)\left(1-\gamma\frac{R_r}{D}\right) dR_r\\
&+ \int_{R_{r1}}^{R_{r2}} 2e^{-j\frac{2\pi}{c_0}F\Delta f_s R_r} R_r I_0\left(\sqrt{w_{DB}^2+z_{DB}^2}\right) dR_r\\
&\left.\left. \times \int_{R_{t1}}^{R_{t2}} e^{-j\frac{2\pi}{c_0}F\Delta f_s R_t} R_t I_0\left(\sqrt{x_{DB}^2+y_{DB}^2}\right)\left(1-\gamma\frac{R_t}{D}\right) dR_t \right] \right.\\
&\left. \times \frac{\eta_{TR}}{I_0(k_T)I_0(k_R)} \frac{\cos\left(\frac{2\pi}{\lambda}\beta_{Rm}d_{Rz}\right)}{1-\left(\frac{4\beta_{Rm}d_{Rz}}{\lambda}\right)^2} \frac{e^{-j2\pi F\Delta f_s D/c_0}}{(R_{t2}^2-R_{t1}^2)(R_{r2}^2-R_{r1}^2)} \right\}\\
&\times \left(\frac{2\pi}{\lambda}d_{Tz}\right) \left[\frac{8\cos\left(\frac{2\pi}{\lambda}\beta_{Tm}d_{Tz}\right)\left(\frac{2\pi}{\lambda}\beta_{Tm}d_{Tz}\right)}{1-8\left(\frac{2\pi}{\lambda}\beta_{Tm}d_{Tz}\right)^2+16\left(\frac{2\pi}{\lambda}\beta_{Tm}d_{Tz}\right)^4} \right.\\
&\left. + \frac{4\left(\frac{2\pi}{\lambda}\beta_{Tm}d_{Tz}\right)^2\sin\left(\frac{2\pi}{\lambda}\beta_{Tm}d_{Tz}\right)-\sin\left(\frac{2\pi}{\lambda}\beta_{Tm}d_{Tz}\right)}{1-8\left(\frac{2\pi}{\lambda}\beta_{Tm}d_{Tz}\right)^2+16\left(\frac{2\pi}{\lambda}\beta_{Tm}d_{Tz}\right)^4} \right] \qquad (54)
\end{aligned}
$$

$$
\begin{aligned}
&[\mathbf{D}_{\Theta_2}(\boldsymbol{\Theta}_{T,F}, T\Delta t_s, F\Delta f_s)]_{q+L_r(p-1),\tilde{q}+L_r(\tilde{p}-1)}\\
&= \frac{\partial R_{pq,\tilde{p}\tilde{q}}^{SBT}(T\Delta t_s, F\Delta f_s)}{\partial k_T} + \frac{\partial R_{pq,\tilde{p}\tilde{q}}^{DB}(T\Delta t_s, F\Delta f_s)}{\partial k_T} = \frac{\eta_T}{I_0(k_T)}\\
&\times \frac{\cos\left(\frac{2\pi}{\lambda}\beta_{Tm}d_{Tz}\right)}{1-\left(\frac{4\beta_{Tm}d_{Tz}}{\lambda}\right)^2} e^{-j\frac{2\pi}{\lambda}(q-\tilde{q})d_{Rx}-j2\pi T\Delta t_s f_{R\max}\cos\gamma_R}\\
&\times \left\{ -\frac{I_1(k_T)}{I_0(k_T)} \int_{R_{t1}}^{R_{t2}} \left(1-\gamma\frac{R_t}{D}\right) e^{-j\frac{2\pi}{c_0}F\Delta f_s(D+R_t)} \frac{2R_t}{R_{t2}^2-R_{t1}^2} \right.\\
&\times I_0\left(\sqrt{x_{SBT}^2+y_{SBT}^2}\right) dR_t + \int_{R_{t1}}^{R_{t2}} \left(1-\gamma\frac{R_t}{D}\right)\\
&\times e^{-j\frac{2\pi}{c_0}\Delta f(D+R_t)} I_1\left(\sqrt{x_{SBT}^2+y_{SBT}^2}\right) \frac{2R_t}{R_{t2}^2-R_{t1}^2}\\
&\left. \times \frac{x_{SBT}\cos\mu_T + y_{SBT}\sin\mu_T}{\sqrt{x_{SBT}^2+y_{SBT}^2}} dR_t \right\} + \frac{\eta_{TR}}{I_0(k_T)I_0(k_R)}\\
&\times \frac{\cos\left(\frac{2\pi}{\lambda}\beta_{Tm}d_{Tz}\right)}{1-\left(\frac{4\beta_{Tm}d_{Tz}}{\lambda}\right)^2} \frac{\cos\left(\frac{2\pi}{\lambda}\beta_{Rm}d_{Rz}\right)}{1-\left(\frac{4\beta_{Rm}d_{Rz}}{\lambda}\right)^2}\\
&\times \frac{e^{-j2\pi F\Delta f_s D/c_0}}{(R_{t2}^2-R_{t1}^2)(R_{r2}^2-R_{r1}^2)}\\
&\times \left\{ -\frac{I_1(k_T)}{I_0(k_T)} \left[\int_{R_{t1}}^{R_{t2}} 2e^{-j\frac{2\pi}{c_0}F\Delta f_s R_t} R_t I_0\left(\sqrt{x_{DB}^2+y_{DB}^2}\right) dR_t \right.\right.\\
&\times \int_{R_{r1}}^{R_{r2}} e^{-j\frac{2\pi}{c_0}F\Delta f_s R_r} R_r I_0\left(\sqrt{w_{DB}^2+z_{DB}^2}\right)\left(1-\gamma\frac{R_r}{D}\right) dR_r\\
&+ \int_{R_{r1}}^{R_{r2}} 2e^{-j\frac{2\pi}{c_0}F\Delta f_s R_r} R_r I_0\left(\sqrt{w_{DB}^2+z_{DB}^2}\right) dR_r\\
&\left.\left. \times \int_{R_{t1}}^{R_{t2}} e^{-j\frac{2\pi}{c_0}F\Delta f_s R_t} R_t I_0\left(\sqrt{x_{DB}^2+y_{DB}^2}\right)\left(1-\gamma\frac{R_t}{D}\right) dR_t \right] \right.\\
&+ \int_{R_{t1}}^{R_{t2}} 2e^{-j\frac{2\pi}{c_0}F\Delta f_s R_t} R_t I_1\left(\sqrt{x_{DB}^2+y_{DB}^2}\right)\\
&\times \frac{x_{DB}\cos\mu_T + y_{DB}\sin\mu_T}{\sqrt{x_{DB}^2+y_{DB}^2}} dR_t\\
&\times \int_{R_{r1}}^{R_{r2}} e^{-j\frac{2\pi}{c_0}F\Delta f_s R_r} R_r I_0\left(\sqrt{w_{DB}^2+z_{DB}^2}\right)\left(1-\gamma\frac{R_r}{D}\right) dR_r\\
&+ \int_{R_{r1}}^{R_{r2}} 2e^{-j\frac{2\pi}{c_0}F\Delta f_s R_r} R_r I_0\left(\sqrt{w_{DB}^2+z_{DB}^2}\right) dR_r\\
&\times \int_{R_{t1}}^{R_{t2}} e^{-j\frac{2\pi}{c_0}F\Delta f_s R_t} R_t I_1\left(\sqrt{x_{DB}^2+y_{DB}^2}\right)\left(1-\gamma\frac{R_t}{D}\right)\\
&\left. \times \frac{x_{DB}\cos\mu_T + y_{DB}\sin\mu_T}{\sqrt{x_{DB}^2+y_{DB}^2}} dR_t \right\} \qquad (55)
\end{aligned}
$$

$$
\begin{aligned}
&[\mathbf{D}_{\Theta_3}(\boldsymbol{\Theta}_{T,F}, T\Delta t_s, F\Delta f_s)]_{q+L_r(p-1),\tilde{q}+L_r(\tilde{p}-1)}\\
&= \frac{\partial R_{pq,\tilde{p}\tilde{q}}^{SBT}(T\Delta t_s, F\Delta f_s)}{\partial \mu_T} + \frac{\partial R_{pq,\tilde{p}\tilde{q}}^{DB}(T\Delta t_s, F\Delta f_s)}{\partial \mu_T} = \frac{\eta_T}{I_0(k_T)}\\
&\times \frac{\cos\left(\frac{2\pi}{\lambda}\beta_{Tm}d_{Tz}\right)}{1-\left(\frac{4\beta_{Tm}d_{Tz}}{\lambda}\right)^2} e^{-j\frac{2\pi}{\lambda}(q-\tilde{q})d_{Rx}-j2\pi T\Delta t_s f_{R\max}\cos\gamma_R}\\
&\times \left\{ \int_{R_{t1}}^{R_{t2}} \left(1-\gamma\frac{R_t}{D}\right) e^{-j\frac{2\pi}{c_0}F\Delta f_s(D+R_t)} I_1\left(\sqrt{x_{SBT}^2+y_{SBT}^2}\right) \right.\\
&\left. \times \frac{y_{SBT}k_T\cos\mu_T - x_{SBT}k_T\sin\mu_T}{\sqrt{x_{SBT}^2+y_{SBT}^2}} \frac{2R_t}{R_{t2}^2-R_{t1}^2} dR_t \right\}\\
&+ \frac{\eta_{TR}}{I_0(k_T)I_0(k_R)} \frac{\cos\left(\frac{2\pi}{\lambda}\beta_{Tm}d_{Tz}\right)}{1-\left(\frac{4\beta_{Tm}d_{Tz}}{\lambda}\right)^2} \frac{\cos\left(\frac{2\pi}{\lambda}\beta_{Rm}d_{Rz}\right)}{1-\left(\frac{4\beta_{Rm}d_{Rz}}{\lambda}\right)^2}\\
&\times \frac{e^{-j2\pi F\Delta f_s D/c_0}}{(R_{t2}^2-R_{t1}^2)(R_{r2}^2-R_{r1}^2)} \left\{ \int_{R_{t1}}^{R_{t2}} 2e^{-j\frac{2\pi}{c_0}F\Delta f_s R_t} R_t \right.
\end{aligned}
$$

$$\times I_1\left(\sqrt{x_{DB}^2+y_{DB}^2}\right)\frac{y_{DB}k_T\cos\mu_T - x_{DB}k_T\sin\mu_T}{\sqrt{x_{DB}^2+y_{DB}^2}}dR_t$$
$$\times\int_{R_{r1}}^{R_{r2}} e^{-j\frac{2\pi}{c_0}F\Delta f_s R_r}R_r I_0\left(\sqrt{w_{DB}^2+z_{DB}^2}\right)\left(1-\gamma\frac{R_r}{D}\right)dR_r$$
$$+\int_{R_{r1}}^{R_{r2}} 2e^{-j\frac{2\pi}{c_0}F\Delta f_s R_r}R_r I_0\left(\sqrt{w_{DB}^2+z_{DB}^2}\right)dR_r$$
$$\times\int_{R_{t1}}^{R_{t2}} e^{-j\frac{2\pi}{c_0}F\Delta f_s R_t}R_t I_1\left(\sqrt{x_{DB}^2+y_{DB}^2}\right)$$
$$\times\frac{y_{DB}k_T\cos\mu_T - x_{DB}k_T\sin\mu_T}{\sqrt{x_{DB}^2+y_{DB}^2}}\left(1-\gamma\frac{R_t}{D}\right)dR_t\Bigg\} \quad (56)$$

$$[\mathbf{D}_{\Theta_4}(\mathbf{\Theta}_{T,F},T\Delta t_s,F\Delta f_s)]_{q+L_r(p-1),\tilde{q}+L_r(\tilde{p}-1)}$$
$$=\frac{\partial R_{pq,\tilde{p}\tilde{q}}^{SBR}(T\Delta t_s,F\Delta f_s)}{\partial\beta_{R_m}}+\frac{\partial R_{pq,\tilde{p}\tilde{q}}^{DB}(T\Delta t_s,F\Delta f_s)}{\partial\beta_{R_m}}$$
$$=\Bigg\{\frac{\eta_R}{I_0(k_R)}\frac{\cos\left(\frac{2\pi}{\lambda}\beta_{Rm}d_{Rz}\right)}{1-\left(\frac{4\beta_{Rm}d_{Rz}}{\lambda}\right)^2}e^{j\frac{2\pi}{\lambda}(p-\tilde{p})d_{Tx}+j2\pi T\Delta t_s f_{T\max}\cos\gamma_T}$$
$$\times\int_{R_{r1}}^{R_{r2}}\left(1-\gamma\frac{R_r}{D}\right)e^{-j\frac{2\pi}{c_0}F\Delta f_s(D+R_r)}I_0\left(\sqrt{x_{SBR}^2+y_{SBR}^2}\right)$$
$$\times\frac{2R_r}{R_{r2}^2-R_{r1}^2}dR_r+\frac{\eta_{TR}}{I_0(k_T)I_0(k_R)}\frac{\cos\left(\frac{2\pi}{\lambda}\beta_{Rm}d_{Rz}\right)}{1-\left(\frac{4\beta_{Rm}d_{Rz}}{\lambda}\right)^2}$$
$$\times\frac{e^{-j2\pi F\Delta f_s D/c_0}}{(R_{t2}^2-R_{t1}^2)(R_{r2}^2-R_{r1}^2)}\Bigg[\int_{R_{t1}}^{R_{t2}}2e^{-j\frac{2\pi}{c_0}F\Delta f_s R_t}R_t$$
$$\times I_0\left(\sqrt{x_{DB}^2+y_{DB}^2}\right)dR_t\int_{R_{r1}}^{R_{r2}}e^{-j\frac{2\pi}{c_0}F\Delta f_s R_r}I_0\left(\sqrt{w_{DB}^2+z_{DB}^2}\right)$$
$$\times R_r\left(1-\gamma\frac{R_r}{D}\right)dR_r+\int_{R_{r1}}^{R_{r2}}2e^{-j\frac{2\pi}{c_0}F\Delta f_s R_r}I_0\left(\sqrt{w_{DB}^2+z_{DB}^2}\right)$$
$$\times R_r dR_r\int_{R_{t1}}^{R_{t2}}e^{-j\frac{2\pi}{c_0}F\Delta f_s R_t}R_t I_0\left(\sqrt{x_{DB}^2+y_{DB}^2}\right)\left(1-\gamma\frac{R_t}{D}\right)$$
$$\times dR_t\Bigg]\Bigg\}\frac{2\pi}{\lambda}d_{Rz}\Bigg[\frac{8\cos\left(\frac{2\pi}{\lambda}\beta_{Rm}d_{Rz}\right)\left(\frac{2\pi}{\lambda}\beta_{Rm}d_{Rz}\right)}{1-8\left(\frac{2\pi}{\lambda}\beta_{Rm}d_{Rz}\right)^2+16\left(\frac{2\pi}{\lambda}\beta_{Rm}d_{Rz}\right)^4}$$
$$+\frac{4\left(\frac{2\pi}{\lambda}\beta_{Rm}d_{Rz}\right)^2\sin\left(\frac{2\pi}{\lambda}\beta_{Rm}d_{Rz}\right)-\sin\left(\frac{2\pi}{\lambda}\beta_{Rm}d_{Rz}\right)}{1-8\left(\frac{2\pi}{\lambda}\beta_{Rm}d_{Rz}\right)^2+16\left(\frac{2\pi}{\lambda}\beta_{Rm}d_{Rz}\right)^4}\Bigg] \quad (57)$$

$$[\mathbf{D}_{\Theta_5}(\mathbf{\Theta}_{T,F},T\Delta t_s,F\Delta f_s)]_{q+L_r(p-1),\tilde{q}+L_r(\tilde{p}-1)}$$
$$=\frac{\partial R_{pq,\tilde{p}\tilde{q}}^{SBR}(T\Delta t_s,F\Delta f_s)}{\partial k_R}+\frac{\partial R_{pq,\tilde{p}\tilde{q}}^{DB}(T\Delta t_s,F\Delta f_s)}{\partial k_R}$$
$$=\frac{\eta_R}{I_0(k_R)}\frac{\cos\left(\frac{2\pi}{\lambda}\beta_{Rm}d_{Rz}\right)}{1-\left(\frac{4\beta_{Rm}d_{Rz}}{\lambda}\right)^2}e^{j\frac{2\pi}{\lambda}(p-\tilde{p})d_{Tx}+j2\pi T\Delta t_s f_{T\max}\cos\gamma_T}$$
$$\times\Bigg\{-\frac{I_1(k_R)}{I_0(k_R)}\int_{R_{r1}}^{R_{r2}}\left(1-\gamma\frac{R_r}{D}\right)e^{-j\frac{2\pi}{c_0}F\Delta f_s(D+R_r)}$$
$$\times\frac{2R_r}{R_{r2}^2-R_{r1}^2}I_0\left(\sqrt{x_{SBR}^2+y_{SBR}^2}\right)dR_r+\int_{R_{r1}}^{R_{r2}}\left(1-\gamma\frac{R_r}{D}\right)$$
$$\times e^{-j\frac{2\pi}{c_0}F\Delta f_s(D+R_r)}I_1\left(\sqrt{x_{SBR}^2+y_{SBR}^2}\right)$$
$$\times\frac{x_{SBR}\cos\mu_R+y_{SBR}\sin\mu_R}{\sqrt{x_{SBR}^2+y_{SBR}^2}}\frac{2R_r}{R_{r2}^2-R_{r1}^2}dR_r\Bigg\}$$
$$+\frac{\eta_{TR}}{I_0(k_T)I_0(k_R)}\frac{\cos\left(\frac{2\pi}{\lambda}\beta_{Tm}d_{Tz}\right)}{1-\left(\frac{4\beta_{Tm}d_{Tz}}{\lambda}\right)^2}\frac{\cos\left(\frac{2\pi}{\lambda}\beta_{Rm}d_{Rz}\right)}{1-\left(\frac{4\beta_{Rm}d_{Rz}}{\lambda}\right)^2}$$
$$\times\frac{e^{-j2\pi F\Delta f_s D/c_0}}{(R_{t2}^2-R_{t1}^2)(R_{r2}^2-R_{r1}^2)}\Bigg\{-\frac{I_1(k_R)}{I_0(k_R)}\Bigg[\int_{R_{t1}}^{R_{t2}}2e^{-j\frac{2\pi}{c_0}F\Delta f_s R_t}R_t$$
$$\times I_0\left(\sqrt{x_{DB}^2+y_{DB}^2}\right)dR_t\int_{R_{r1}}^{R_{r2}}e^{-j\frac{2\pi}{c_0}F\Delta f_s R_r}I_0\left(\sqrt{w_{DB}^2+z_{DB}^2}\right)$$
$$\times R_r\left(1-\gamma\frac{R_r}{D}\right)dR_r+\int_{R_{r1}}^{R_{r2}}2e^{-j\frac{2\pi}{c_0}F\Delta f_s R_r}I_0\left(\sqrt{w_{DB}^2+z_{DB}^2}\right)$$
$$\times R_r dR_r\int_{R_{t1}}^{R_{t2}}e^{-j\frac{2\pi}{c_0}F\Delta f_s R_t}R_t I_0\left(\sqrt{x_{DB}^2+y_{DB}^2}\right)$$
$$\times\left(1-\gamma\frac{R_t}{D}\right)dR_t\Bigg]+\int_{R_{t1}}^{R_{t2}}2e^{-j\frac{2\pi}{c_0}F\Delta f_s R_t}I_0\left(\sqrt{x_{DB}^2+y_{DB}^2}\right)$$
$$\times R_t dR_t\int_{R_{r1}}^{R_{r2}}e^{-j\frac{2\pi}{c_0}F\Delta f_s R_r}R_r\frac{z_{DB}\cos\mu_R+w_{DB}\sin\mu_R}{\sqrt{z_{DB}^2+w_{DB}^2}}$$
$$\times I_1\left(\sqrt{w_{DB}^2+z_{DB}^2}\right)\left(1-\gamma\frac{R_r}{D}\right)dR_r+\int_{R_{r1}}^{R_{r2}}2e^{-j\frac{2\pi}{c_0}F\Delta f_s R_r}$$
$$\times R_r I_1\left(\sqrt{w_{DB}^2+z_{DB}^2}\right)\frac{z_{DB}\cos\mu_R+w_{DB}\sin\mu_R}{\sqrt{z_{DB}^2+w_{DB}^2}}dR_r$$
$$\times\int_{R_{t1}}^{R_{t2}}e^{-j\frac{2\pi}{c_0}F\Delta f_s R_t}R_t I_0\left(\sqrt{x_{DB}^2+y_{DB}^2}\right)\left(1-\gamma\frac{R_t}{D}\right)dR_t\Bigg\} \quad (58)$$

$$[\mathbf{D}_{\Theta_6}(\mathbf{\Theta}_{T,F},T\Delta t_s,F\Delta f_s)]_{q+L_r(p-1),\tilde{q}+L_r(\tilde{p}-1)}$$
$$=\frac{\partial R_{pq,\tilde{p}\tilde{q}}^{SBR}(T\Delta t_s,F\Delta f_s)}{\partial\mu_R}+\frac{\partial R_{pq,\tilde{p}\tilde{q}}^{DB}(T\Delta t_s,F\Delta f_s)}{\partial\mu_R}$$
$$=\frac{\eta_R}{I_0(k_R)}\frac{\cos\left(\frac{2\pi}{\lambda}\beta_{Rm}d_{Rz}\right)}{1-\left(\frac{4\beta_{Rm}d_{Rz}}{\lambda}\right)^2}e^{j\frac{2\pi}{\lambda}(p-\tilde{p})d_{Tx}+j2\pi T\Delta t_s f_{T\max}\cos\gamma_T}$$

$$\times \left\{ \int_{R_{r1}}^{R_{r2}} \left(1-\gamma\frac{R_r}{D}\right) e^{-j\frac{2\pi}{c_0}F\Delta f_s(D+R_r)} I_1\left(\sqrt{x_{SBR}^2+y_{SBR}^2}\right) \right.$$

$$\left. \times \frac{y_{SBR}k_R\cos\mu_R - x_{SBR}k_R\sin\mu_R}{\sqrt{x_{SBR}^2+y_{SBR}^2}} \frac{2R_r}{R_{r2}^2-R_{r1}^2} dR_r \right\}$$

$$+ \frac{\eta_{TR}}{I_0(k_T)I_0(k_R)} \frac{\cos\left(\frac{2\pi}{\lambda}\beta_{Tm}d_{Tz}\right)}{1-\left(\frac{4\beta_{Tm}d_{Tz}}{\lambda}\right)^2} \frac{\cos\left(\frac{2\pi}{\lambda}\beta_{Rm}d_{Rz}\right)}{1-\left(\frac{4\beta_{Rm}d_{Rz}}{\lambda}\right)^2}$$

$$\times \frac{e^{-j2\pi F\Delta f_s D/c_0}}{\left(R_{t2}^2-R_{t1}^2\right)\left(R_{r2}^2-R_{r1}^2\right)} \left\{ \int_{R_{t1}}^{R_{t2}} 2e^{-j\frac{2\pi}{c_0}F\Delta f_s R_t} R_t \right.$$

$$\times I_0\left(\sqrt{x_{DB}^2+y_{DB}^2}\right) dR_t \int_{R_{r1}}^{R_{r2}} e^{-j\frac{2\pi}{c_0}F\Delta f_s R_r} R_r$$

$$\times I_1\left(\sqrt{w_{DB}^2+z_{DB}^2}\right) \frac{w_{DB}k_R\cos\mu_R - z_{DB}k_R\sin\mu_R}{\sqrt{w_{DB}^2+z_{DB}^2}}$$

$$\times \left(1-\gamma\frac{R_r}{D}\right) dR_r + \int_{R_{r1}}^{R_{r2}} 2e^{-j\frac{2\pi}{c_0}F\Delta f_s R_r} R_r I_1\left(\sqrt{w_{DB}^2+z_{DB}^2}\right)$$

$$\times \frac{w_{DB}k_R\cos\mu_R - z_{DB}k_R\sin\mu_R}{\sqrt{z_{DB}^2+w_{DB}^2}} dR_r$$

$$\times \int_{R_{t1}}^{R_{t2}} e^{-j\frac{2\pi}{c_0}F\Delta f_s R_t} R_t I_0\left(\sqrt{x_{DB}^2+y_{DB}^2}\right)\left(1-\gamma\frac{R_t}{D}\right) dR_t \quad (59)$$

$$[\mathbf{D}_{\Theta_7}(\mathbf{\Theta}_{T,F}, T\Delta t_s, F\Delta f_s)]_{q+L_R(p-1),\tilde{q}+L_R(\tilde{p}-1)}$$

$$= \frac{\partial R_{pq,\tilde{p}\tilde{q}}^{SBT}(T\Delta t_s, F\Delta f_s)}{\partial \eta_T} + \frac{\partial R_{pq,\tilde{p}\tilde{q}}^{DB}(T\Delta t_s, F\Delta f_s)}{\partial \eta_T}$$

$$= \frac{1}{I_0(k_T)} \frac{\cos\left(\frac{2\pi}{\lambda}\beta_{Tm}d_{Tz}\right)}{1-\left(\frac{4\beta_{Tm}d_{Tz}}{\lambda}\right)^2} e^{-j\frac{2\pi}{\lambda}(q-\tilde{q})d_{Rx} - j2\pi T\Delta t_s f_{R\max}\cos\gamma_R}$$

$$\times \int_{R_{t1}}^{R_{t2}} \left(1-\gamma\frac{R_t}{D}\right) e^{-j\frac{2\pi}{c_0}F\Delta f_s(D+R_t)} I_0\left(\sqrt{x_{SBT}^2+y_{SBT}^2}\right)$$

$$\times \frac{2R_t}{R_{t2}^2-R_{t1}^2} dR_t - \frac{1}{I_0(k_T)I_0(k_R)} \frac{\cos\left(\frac{2\pi}{\lambda}\beta_{Tm}d_{Tz}\right)}{1-\left(\frac{4\beta_{Tm}d_{Tz}}{\lambda}\right)^2}$$

$$\times \frac{\cos\left(\frac{2\pi}{\lambda}\beta_{Rm}d_{Rz}\right)}{1-\left(\frac{4\beta_{Rm}d_{Rz}}{\lambda}\right)^2} \frac{e^{-j2\pi F\Delta f_s D/c_0}}{\left(R_{t2}^2-R_{t1}^2\right)\left(R_{r2}^2-R_{r1}^2\right)}$$

$$\times \left\{ \int_{R_{t1}}^{R_{t2}} 2e^{-j\frac{2\pi}{c_0}F\Delta f_s R_t} R_t I_0\left(\sqrt{x_{DB}^2+y_{DB}^2}\right) dR_t \right.$$

$$\times \int_{R_{r1}}^{R_{r2}} e^{-j\frac{2\pi}{c_0}F\Delta f_s R_r} R_r I_0\left(\sqrt{w_{DB}^2+z_{DB}^2}\right)\left(1-\gamma\frac{R_r}{D}\right) dR_r$$

$$\left. + \int_{R_{r1}}^{R_{r2}} 2e^{-j\frac{2\pi}{c_0}F\Delta f_s R_r} R_r I_0\left(\sqrt{w_{DB}^2+z_{DB}^2}\right) dR_r \right.$$

$$\left. \times \int_{R_{t1}}^{R_{t2}} e^{-j\frac{2\pi}{c_0}F\Delta f_s R_t} R_t I_0\left(\sqrt{x_{DB}^2+y_{DB}^2}\right)\left(1-\gamma\frac{R_t}{D}\right) dR_t \right\} \quad (60)$$

$$[\mathbf{D}_{\Theta_8}(\mathbf{\Theta}_{T,F}, T\Delta t_s, F\Delta f_s)]_{q+L_r(p-1),\tilde{q}+L_r(\tilde{p}-1)}$$

$$= \frac{\partial R_{pq,\tilde{p}\tilde{q}}^{SBR}(T\Delta t_s, F\Delta f_s)}{\partial \eta_R} + \frac{\partial R_{pq,\tilde{p}\tilde{q}}^{DB}(T\Delta t_s, F\Delta f_s)}{\partial \eta_R}$$

$$= \frac{1}{I_0(k_R)} \frac{\cos\left(\frac{2\pi}{\lambda}\beta_{Rm}d_{Rz}\right)}{1-\left(\frac{4\beta_{Rm}d_{Rz}}{\lambda}\right)^2} e^{j\frac{2\pi}{\lambda}(p-\tilde{p})d_{Tx} + j2\pi T\Delta t_s f_{T\max}\cos\gamma_T}$$

$$\times \int_{R_{r1}}^{R_{r2}} \left(1-\gamma\frac{R_r}{D}\right) e^{-j\frac{2\pi}{c_0}F\Delta f_s(D+R_r)} I_0\left(\sqrt{x_{SBR}^2+y_{SBR}^2}\right)$$

$$\times \frac{2R_r}{R_{r2}^2-R_{r1}^2} dR_r - \frac{1}{I_0(k_T)I_0(k_R)} \frac{\cos\left(\frac{2\pi}{\lambda}\beta_{Tm}d_{Tz}\right)}{1-\left(\frac{4\beta_{Tm}d_{Tz}}{\lambda}\right)^2}$$

$$\times \frac{\cos\left(\frac{2\pi}{\lambda}\beta_{Rm}d_{Rz}\right)}{1-\left(\frac{4\beta_{Rm}d_{Rz}}{\lambda}\right)^2} \frac{e^{-j2\pi F\Delta f_s D/c_0}}{\left(R_{t2}^2-R_{t1}^2\right)\left(R_{r2}^2-R_{r1}^2\right)}$$

$$\times \left\{ \int_{R_{t1}}^{R_{t2}} 2e^{-j\frac{2\pi}{c_0}F\Delta f_s R_t} R_t I_0\left(\sqrt{x_{DB}^2+y_{DB}^2}\right) dR_t \right.$$

$$\times \int_{R_{r1}}^{R_{r2}} e^{-j\frac{2\pi}{c_0}F\Delta f_s R_r} R_r I_0\left(\sqrt{w_{DB}^2+z_{DB}^2}\right)\left(1-\gamma\frac{R_r}{D}\right) dR_r$$

$$+ \int_{R_{r1}}^{R_{r2}} 2e^{-j\frac{2\pi}{c_0}F\Delta f_s R_r} R_r I_0\left(\sqrt{w_{DB}^2+z_{DB}^2}\right) dR_r$$

$$\left. \times \int_{R_{t1}}^{R_{t2}} e^{-j\frac{2\pi}{c_0}F\Delta f_s R_t} R_t I_0\left(\sqrt{x_{DB}^2+y_{DB}^2}\right)\left(1-\gamma\frac{R_t}{D}\right) dR_t \right\}. \quad (61)$$

Finally, the CRLB of the estimated parameter Θ_i is the diagonal element of the inverse Fisher information matrix that corresponds to the parameter Θ_i.

ACKNOWLEDGMENT

The authors would like to thank the anonymous reviewers, whose feedback helped improve the quality of this paper.

REFERENCES

[1] A. S. Akki and F. Haber, "A statistical model of mobile-to-mobile land communication channel," *IEEE Trans. Veh. Technol.*, vol. VT-35, no. 1, pp. 2–10, Feb. 1986.

[2] R. Wang and D. Cox, "Channel modeling for ad hoc mobile wireless networks," in *Proc. IEEE VTC*, Birmingham, AL, May 2002, vol. 1, pp. 21–25.

[3] C. S. Patel, G. L. Stüber, and T. G. Pratt, "Simulation of Rayleigh-faded mobile-to-mobile communication channels," *IEEE Trans. Commun.*, vol. 53, no. 10, pp. 1876–1884, Oct. 2005.

[4] A. G. Zajić and G. L. Stüber, "A new simulation model for mobile-to-mobile Rayleigh fading channels," in *Proc. IEEE WCNC*, Las Vegas, NV, Apr. 2006, vol. 3, pp. 1266–1270.

[5] J. Maurer, T. Fügen, and W. Wiesbeck, "Narrow-band measurement and analysis of the intervehicle transmission channel at 5.2 GHz," in *Proc. IEEE VTC*, Birmingham, AL, May 2002, pp. 1274–1278.

[6] G. Acosta and M. A. Ingram, "Model development for the wideband expressway vehicle-to-vehicle 2.4-GHz channel," in *Proc. IEEE WCNC*, Las Vegas, NV, Apr. 2006, vol. 3, pp. 1283–1288.
[7] M. Pätzold, B. O. Hogstad, N. Youssef, and D. Kim, "A MIMO mobile-to-mobile channel model: Part I—The reference model," in *Proc. IEEE PIMRC*, Berlin, Germany, Sep. 2005, vol. 1, pp. 573–578.
[8] B. O. Hogstad, M. Pätzold, N. Youssef, and D. Kim, "A MIMO mobile-to-mobile channel model: Part II—The simulation model," in *Proc. IEEE PIMRC*, Berlin, Germany, Sep. 2005, vol. 1, pp. 562–567.
[9] A. G. Zajić and G. L. Stüber, "A three-dimensional parametric model for wideband MIMO mobile-to-mobile channels," in *Proc. IEEE GLOBECOM*, Washington, DC, Nov. 2007, pp. 3760–3764.
[10] A. G. Zajić and G. L. Stüber, "Three-dimensional modeling and simulation of wideband MIMO mobile-to-mobile channels," *IEEE Trans. Wireless Commun*. submitted for publication.
[11] A. G. Zajić and G. L. Stüber"Statistical properties of wideband MIMO mobile-to-mobile channels," in *Proc. IEEE WCNC*, Las Vegas, NV, Apr. 2008, pp. 763–768.
[12] A. G. Zajić and G. L. Stüber, "3-D simulation models for wideband MIMO mobile-to-mobile channels," in *Proc. IEEE MILCOM*, Orlando, FL, Oct. 2007, pp. 1–5.
[13] C. B. Ribeiro, E. Ollila, and V. Koivunen, "Stochastic maximum likelihood method for propagation parameter estimation," in *Proc. IEEE PIMRC*, Sep. 2004, vol. 3, pp. 1839–1843.
[14] D. Gesbert, H. Bölcskei, D. A. Gore, and A. J. Paulraj, "Outdoor MIMO wireless channels: models and performance prediction," *IEEE Trans. Commun.*, vol. 50, no. 12, pp. 1926–1934, Dec. 2002.
[15] J. G. Proakis, *Digital Communications*, 4th ed. New York: McGraw-Hill, 2001.
[16] A. Abdi, J. A. Barger, and M. Kaveh, "A parametric model for the distribution of the angle of arrival and the associated correlation function and power spectrum at the mobile station," *IEEE Trans. Veh. Technol.*, vol. 51, no. 3, pp. 425–434, May 2002.
[17] J. D. Parsons and A. M. D. Turkmani, "Characterization of mobile radio signals: Model description," *Proc. Inst. Elect. Eng.—I, Commun., Speech, Vis.*, vol. 138, no. 6, pp. 549–556, Dec. 1991.
[18] A. Kuchar, J.-P. Rossi, and E. Bonek, "Directional macrocell channel characterization from urban measurements," *IEEE Trans. Antennas Propag.*, vol. 48, no. 2, pp. 137–146, Feb. 2000.
[19] W. C. Y. Lee, "Estimate of local average power of a mobile radio signal," *IEEE Trans. Veh. Technol.*, vol. VT-34, no. 1, pp. 22–27, Feb. 1985.
[20] P. D. Welch, "The use of fast Fourier transform for the estimation of power spectra: A method based on time averaging over short, modified periodograms," *IEEE Trans. Audio Electroacoust.*, vol. AU-15, no. 2, pp. 70–73, Jun. 1967.
[21] L. J. Greenstein, D. G. Michelson, and V. Erceg, "Moment-method estimation of the Ricean K-factor," *IEEE Commun. Lett.*, vol. 3, no. 6, pp. 175–176, Jun. 1999.
[22] R. Fletcher, *Practical Methods of Optimization—Constrained Optimization*, 2nd ed. Hoboken, NJ: Wiley, 1981.
[23] M. Pätzold, U. Killat, and F. Laue, "An extended Suzuki model for land mobile satellite channels and its statistical properties," *IEEE Trans. Veh. Technol.*, vol. 47, no. 2, pp. 617–630, May 1998.
[24] G. L. Stüber, *Principles of Mobile Communication*, 2nd ed. Norwell, MA: Kluwer, 2001.

Alenka G. Zajić (S'99) received the B.Sc. and M.Sc. degrees from the University of Belgrade, Belgrade, Serbia, in 2001 and 2003, respectively. She is currently working toward the Ph.D. degree with the School of Electrical and Computer Engineering, Georgia Institute of Technology, Atlanta.

From 2001 to 2003, she was a Design Engineer with Skyworks Solutions Inc., Fremont, CA. Since 2004, she has been a Graduate Research Assistant with the Wireless Systems Laboratory, School of Electrical and Computer Engineering, Georgia Institute of Technology. Her research interests include wireless communications and applied electromagnetics.

Ms. Zajić received the 2004 Dan Noble Fellowship from Motorola Inc. and the IEEE Vehicular Technology Society for her work on quality impact in vehicular technology.

Gordon L. Stüber (S'81–M'82–SM'96–F'99) received the B.A.Sc. and Ph.D. degrees in electrical engineering from the University of Waterloo, Waterloo, ON, Canada, in 1982 and 1986, respectively.

Since 1986, he has been with the School of Electrical and Computer Engineering, Georgia Institute of Technology, Atlanta, where he is currently the Joseph M. Pettit Chair in Communications. He is the author of *Principles of Mobile Communication* (Kluwer, 1996, 2nd ed., 2001). His research interests include wireless communication systems and communications signal processing.

Dr. Stüber was the Technical Program Chair of the 46th IEEE Vehicular Technology Conference (VTC 1996) and the 1998 IEEE International Conference on Communications (ICC) and the General Chair of the Fifth IEEE Workshop on Multimedia, Multiaccess, and Teletraffic for Wireless Communications (MMT 2000), the 31st Annual IEEE Communication Theory Workshop (CT 2002), and the Fifth International Symposium on Wireless Personal Multimedia Communications (WPMC 2002). From 1993 to 1998, he was an Editor for Spread Spectrum of the IEEE TRANSACTIONS ON COMMUNICATIONS. From 1999 to 2002, he was a member of the IEEE Communications Society Awards Committee. He is currently a Member-at-Large of the IEEE Vehicular Technology Society Board of Governors and the IEEE Communications Society Board of Governors. He was a corecipient of the 1997 Jack Neubauer Memorial Award, which recognizes the best systems paper published in the IEEE TRANSACTIONS ON VEHICULAR TECHNOLOGY. He received the IEEE Vehicular Technology Society James R. Evans Avant Garde Award in 2003 for his contributions to theoretical research in wireless communications and the IEEE Vehicular Technology Society Outstanding Service Award in 2005.

Thomas G. Pratt (M'97) received the B.S. degree in electrical engineering from the University of Notre Dame, Notre Dame, IN, in 1981 and the M.S. and Ph.D. degrees from the Georgia Institute of Technology (Georgia Tech), Atlanta, in 1989 and 1999, respectively.

Since 1985, he has been a full-time Research Engineer with the Georgia Tech Research Institute, where he currently heads the Software Radio Laboratory and leads research in channel modeling, multiple-input–multiple-output systems, and interference suppression. His research work is focused on wireless communications.

Son T. Nguyen received the B.S.E.E. degree from the University of South Florida, Tampa, in 1982 and the M.S.E.E. degree from Fairleigh Dickinson University, Hackensack, NJ, in 1987.

Since 1983, he has been with the U.S. Army through various commands and is currently with the Army Research Laboratory, Adelphi, MD. He is engaged with the Software Radio Laboratory, Georgia Tech Research Institute, Georgia Institute of Technology, Atlanta, under the CTA Rotational Research Program. His research interests include wired and wireless communications, network security, modeling, and simulation.